Tectonic Setting and Geochemistry of Submarine Volcanics from the Northern Termination of the Tonga Arc: Implications for the Involvement of Samoan Mantle Plume in Arc-Backarc Magmatism

Trevor J. Falloon
School of Earth Sciences and Centre for Marine Sciences, UTas, GPO Box 252-79, Hobart, Tasmania 7001, Australia (trevor.falloon@utas.edu.au)

Leonid V. Danyushevsky, and Tony J. Crawford
Centre for Ore Deposit Research and School of Earth Sciences, UTas, GPO Box 252-79, Hobart, Tasmania 7001, Australia (l.Dan@utas.edu.au; tony.crawford@utas.edu.au)

Roland Maas, and Jon D. Woodhead
School of Earth Sciences, University of Melbourne, Victoria 3010, Australia (maasr@unimelb.edu.au; jdwood@unimelb.edu.au)

Stephen M. Eggins
Research School of Earth Sciences, The Australian National University, Canberra, ACT 0200, Australia (stephen.eggins@anu.edu.au)

Sherman H. Bloomer, and Dawn J. Wright
Department of Geosciences, Oregon State University, Corvallis, OR 97331-5506, USA (sherman.bloomer@oregonstate.edu; dawn@dusk.geo.orst.edu)

Sergei K. Zlobin
Vernadsky Institute of Geochemistry and Analytical Chemistry, Russian Academy of Sciences, 19 Kosygina Str, 117975, Moscow, Russia (lions@aha.ru)

Andrew R. Stacey
School of Earth Sciences, UTas, GPO Box 252-79, Hobart, Tasmania 7001, Australia (arstacey@utas.edu.au)

[1] New seafloor mapping and sampling demonstrates that the eruption of the high-Ca boninites is clearly associated with rifting of the northern Tonga ridge and the northern Lau Basin at the northern termination of the Tonga Trench. There is very strong evidence for OIB plume related mantle sources involved in the petrogenesis of lavas erupted in the northern Lau Basin and at the termination of north Tonga ridge. Evidence comes from 1) geophysics, which indicates there is a deep flow of mantle across the 'slab window' formed by the trench- transform fault transition 2) geochemistry of boninites

and associated rift related lavas which display strongly LREE enriched patterns, enrichment in HFSE such as Nb and Ta and low ^{143}Nd/^{144}Nd isotope values and 3) petrogenetic conditions of Tongan boninites, whose primary magmas have ~24 wt% MgO, require refractory lherzolite-harzburgite sources and temperates of at least ~1480°C at 1.5 Gpa. The presence of abnormally hot mantle at relatively shallow depths at the northern Tonga ridge, results from intrusion of a hot refractory OIB Samoan plume mantle source into the mantle wedge. The isotope results from this study supports the view that mantle mixing between Samoan plume mantle and an Indian-type mantle source beneath northern Lau Basin is the dominant influence on isotope compositions of lavas erupted in the northern Lau Basin, including the island of Niua Fo'ou. However the source mantle of the active Tofua Arc is more consistent with mixing between a Pacific-type mantle source and material derived from the Society Island plume. It is speculated that mantle flow through the slab 'window' at the northern termination of the Tonga Trench is relatively long-lived (at least as old as the earliest of Lau Basin opening) which has allowed a range of source components to mix with mantle sources involved in Lau back-arc magma genesis.

Components: 7,647 words, 16 figures, 7 tables, 3 appendixes

Keywords: high-Ca boninites; Sr-Nd-Pb isotopes; Samoa, Tonga, Lau Basin, Trench-Transform intersection.

Index Terms: 3001 Back-arc basin processes; 3039 Oceanic transform and fracture zone processes; 3613 Subduction zone processes; 3075 Submarine tectonics and volcanism; 3619 Magma genesis and partial melting.

1. Introduction

[2] At the northern termination of the Tonga Trench and northern Lau Basin (Figures 1-4) a wide variety of high-Ca boninite and tholeiitic magmas have been recovered by rock dredging or submersible sampling by four research vessels: 1) voyage 16 of the R/V Kallisto in 1982 [*Sharaskin et al.,* 1983]; 2) the 1984 voyage of the R/V Natsushima [*Falloon et al.,* 1987]; 3) the 1990 voyage of the R/V Keldysh/Mir [*Falloon et al*., 1992] and 4) the 1996 voyage of the R/V Melville [Boomerang Leg 8, May to June 1996, BMRG08MV, *Bloomer et al.,* 1996; *Falloon et al.,* 1997; *Wright et al.,* 2000]. During BMRG08MV the termination of the northern Tonga Trench was mapped using the Sea Beam 2000 multibeam swath mapping system [*Wright et al.,* 2000; Figures 2-4]. This sea-floor mapping has for the first time provided information on the detailed geological and tectonic context of the high-Ca boninites recovered on research cruises prior to 1996. The main aim of this paper, therefore, is to present new geochemical results on rock samples recovered by dredging during BMRG08MV and to provide a synthesis of older data in the context of the new seafloor mapping of this area. We also present new ICPMS and Nd, Sr and Pb isotope geochemistry for key samples from pre-1996 voyages in this area, which are used together with our new data from the Melville voyage to provide better constraints to our understanding of the petrogenesis of high-Ca boninite magmas at the northern termination of the Tonga Trench and forearc.

2. Geological Setting and Dredge Locations

[3] The location of our study area and general tectonic features are shown schematically in Figure 1. The Tonga intra-oceanic arc is recognized as a type example of an extension-dominated, non-accretionary convergent margin [*Tappin,* 1994; Tappin *et al.,* 1994; *MacLeod*, 1996], with active extensional tectonism throughout the forearc and landward trench slopes. The Tonga Trench is the site of westward subduction of the Pacific Plate beneath the northeastern corner of the Australian Plate. Recently *Zellmer and Taylor* [2001] on the basis of detailed study of acoustic reflectivity and morphology have identified three microplates to explain the kinematics of the Lau Basin – Tonga Trench system in the northern part of the Lau Basin. The three plates identified (Figure 1) are named the Niuafo'ou Plate, the Tonga Plate and the Australian Plate itself, in the southern part of the Lau Basin. The Peggy Ridge in the Northern Lau Basin marks the Southern boundary between the Australian and Niua fo'ou Plates. As will be discussed later, the Peggy Ridge is a geochemical boundary separating Indian like MORB mantle erupting in the Southern Lau Basin from Samoan plume contaminated mantle which appears to characterize magmas associated with the Niua fo'ou Plate and Niua fo'ou Island itself.

[4] GPS measurements indicate that the instantaneous plate convergence across the northern Tonga Trench is 24 cm/yr, the fastest recorded convergence velocity on the modern Earth [*Bevis et al.,* 1995]. At the northern terminus of the trench near 15°S (Figure 1), plate convergence gives way to complex strike-slip motion along a transform fault and back-arc extension in the northern Lau Basin. The trench-transform fault transition forms a slab-edge, the geometric consequences of which are the on-going rupture and rifting of oceanic lithosphere [*Govers and Wortel*, 2005; *Millen and Hamburger*, 1998]. The tearing of the Pacific plate at the northern terminus of the Tonga Trench (Figure 2) is evident at 15° - 16° S where the landward trench slope steepens significantly, the forearc narrows, and the trench axis is 'pinched' by the presence of the Uo Mamae seamount. The Pacific Plate displays striking WNW-trending lineaments which are interpreted by *Wright et al.* [2000] to be older Pacific Plate structures that have been reactivated by hinge-faulting at the bend in the trench.

[5] A consequence of the slab edge is the presence of a 'slab window' which has allowed the flow of hot mantle from the Samoan plume into the northern Lau Basin above the subducting Pacific Plate [*Danyushevsky et al.,* 1995; *Smith et al.,* 2001; *Millen and Hamburger*, 1998]. Hot refractory Samoan mantle fluxed by slab-derived fluids is the primary cause for the presence of high-Ca boninite magmas at the termination of the Tonga Trench and northern Lau Basin [*Danyushevsky et al.,* 1995].

[6] Seabeam mapping along this boundary and the termination of the trench (Figures 2-4), reveals a tectonically complex terrain, including the transition from subduction to strike-slip motion, and the north- and southeast limbs of the Kings Triple Junction [KTJ, also known as the Mangatolu Triple Junction; *Zellmer and Taylor*, 2001]. This terrain contains: 1) new seafloor generated by backarc spreading; 2) deep well-defined graben

structure cutting across the Tonga Arc crust; 3) extensional rift zones associated with large caldera-like features; and 4) young volcanic seamounts located within extensional and graben structures.

[7] Locations from dredging or submersible sampling from the Kallisto, Kelydsh, Natsushima voyages are presented in Figures 2 and 3. Dredging results from the Melville cruise are summarized in Table 1 and also presented in Figures 2 and 3. Available radiometric age dating of rocks from the area are presented in Table 2. Brief petrographic descriptions and mineral chemistry of the samples collected from the Melville cruise are presented in Appendixes 1 and 2. In appendix 3 we present the corrected data of *Falloon and Crawford* [1991].

[8] The sampling covers seven specific tectono-magmatic elements of the northern Lau Basin-Tonga Trench termination as outlined below moving west to east in Figures 2 and 3. Radiometric ages and radiogenic isotope analyses from a number of samples from both the Keldysh and Kallisto cruises are reported by *Acland* [1996].

2.1. Inner-slope of the westernmost extent of the Tonga trench

[9] During the 1982 voyage of the R/V Kallisto fresh pillow lavas were recovered from stations 16-9 and 16-10 [*Sharaskin et al.,* 1983; *Zlobin et al.,* 1991] located within a backarc rift zone associated with the transition from a trench to a transform plate boundary in this area.

2.2. Northeastern spreading arm of the Kings Triple Junction

[10] The mapping reveals a nascent spreading center (Figure 3, the location is identified by dredge D120), featuring a series of parallel, or closely-spaced ridges and troughs. The spreading center can be clearly identified to within about 30km of the trench axis and it is likely that the spreading center intersection with the trench forms a ridge-transform-transform triple junction between the Tonga Plate, the Pacific Plate and the Niuafo'ou Plate. This spreading center is a continuation of the northeastern limb of the Kings Triple Junction (Figure 2, M-2212, M-2218, M-2216), a back-arc ridge-ridge-ridge junction. The Kings Triple Junction is located ~15° 37'S, 174° 52' W, and is characterized by intense deformation and neovolcanism [*Parson and Tiffin*, 1993].

[11] The detailed geological structure of the Lau Basin including the KTJ is presented by *Zellmer and Taylor*, [2001]. During the 1990 voyage of the R/V Kelydsh, three Mir dives were conducted on the KTJ. Two dives [M-2212, M-2218; *Falloon et al.,* 1992] were conducted close to the center of the triple junction, and one dive [M-2216; *Falloon et al.,* 1992] was conducted on the northeastern branch of the triple junction (Fig.2). During voyage BMRG08MV one dredge (D120, Table 1, Figure 2) was conducted on the northeastern end of this branch which also intersects the Tonga Trench to form another triple junction [*Wright et al.,* 2000].

2.3. Back-arc caldera

[12] To the south of D120 (~50 km) and on the eastern side of the spreading ridge lies a 10km wide caldera with a significant breach on its southern rim (Figure 3, D116-117). Dredges 116 and 117 (Table 1) were conducted respectively on the central volcanic cone and eastern wall of this large back-arc caldera (Figures 2-4).

2.4. Rift related boninite lavas – 'western group boninites'

[13] The seabeam mapping reveals that the boninites sampled during voyage 16 of the R/V Kallisto in 1982 [stations 26 (samples 26-1 and 26-2) and the 1984 voyage of the R/V Natsushima in 1984 [Stations 24 (sample 6-3) and 25 (sample 7-18)] were derived from young volcanic cones associated with a rift graben immediately to the east of the spreading center sampled by D120. The cones are young based on their undisturbed shape despite being in a tectonically active area, lack of alteration and Mn coating on pillow rinds of the erupted lavas and radiometric dating [Table 2, *Falloon et al.,* 1987; *Acland,* 1996]. These boninites, along with station 16-28, were referred to as the 'western group' boninites by *Sobolev and Danyushevsky* [1994] and *Danyushevsky et al.* [1995]. During the 1996 Melville voyage D119 (Table 1) was conducted on a small volcanic cone on the western side of the rift graben where boninite lavas were also recovered.

2.5. Tonga Trench at the northern termination of the Tofua Volcanic Arc

[14] Boninite lavas were recovered at station 16-51 (Kallisto), station 21 (Natsushima) and D113 (Melville) from this area (Figure 3, Table 1). The boninites from this area belong to the 'Eastern group' boninites of *Sobolev and Danyushevsky* [1994] and *Danyushevsky et al.* [1995]. The radiometric ages obtained for boninites from station 16-51 and station 21 give relatively young ages (~1-3Ma, Table 2) which overlap the age of modern Tofua Arc volcanism on the islands of Tamari and Niuatoputapu (Table 2).

2.6. Large rift graben cutting the north Tonga ridge at its northern termination

[15] This rift graben was first identified by the Natsushima voyage which sampled the north facing wall of the graben at station 23 [*Falloon et al.,* 1987]. During the Melville cruise the rift wall was again sampled by D115 and boninite lavas recovered (Table 2). Also sampled at D118 was a large submarine volcanic edifice which completely fills the central part of the graben (Figures 3 and 4). Boninites from this rift graben are also part of the 'eastern group' boninites.

2.7. Uo Mamae seamount

[16] The Kallisto voyage sampled the most southerly seamount of the Samoan plume, Uo Mamae [16-94 to 16-100, *Sharaskin et al.,* 1983]. This seamount is starting to be pulled apart by the rifting of the Pacific Plate at the termination of the Tonga Trench [*Wright et al.*, 2000]. We have analysed sample 16-94/1 for trace elements using ICPMS.

3. Analytical Techniques

[17] Major and trace element analyses of rocks dredged during the Melville 1996 voyage are presented in Table 3 and were performed at the School of Earth Sciences (UTAS) using X-ray fluorescence spectrometry (XRF) and the methods of *Robinson et al.* [2003]. Electron Microprobe Probe Analysis (EMPA) of interstial glass and pillow rind glass are presented in Table 4 and were obtained using a Cameca SX50 electron microprobe at the Central Science laboratory, University of Tasmania, Hobart, at 15 kV and 20 ηA, using international standard USNM 111240/2 (basaltic glass) from *Jarosewich et al.* [1980]. Additional trace element geochemistry (Table 5) was obtained by Inductively-coupled Plasma-Mass Spectrometry (ICPMS) at three different laboratories as follows: 1) School of Earth Sciences and Central Science Laboratories (UTAS) using the methods of *Robinson et al.* [1999] and *Yu et al.* [2000]; 2) Research School of Earth Sciences, Australian National University using the method of *Eggins et al.* [1997]; Department of Earth Sciences, University of Bristol (A.J.Kemp analyst). Isotope analyses (Table 6) were obtained from three different laboratories as follows: 1) University of Melbourne using the techniques outlined in *Kamenetsky and Maas* [2002]; 2) Australian National University (J. Woodhead analyst) and 3) University of Adelaide (J. Foden analyst).

4. RESULTS

4.1. Previous work on Tongan high-Ca boninites

[18] Boninites are an important 'end-member' supra-subduction zone magmatic suite as they have the highest H_2O contents and require the most refractory of mantle wedge sources. They are characterized by relatively high SiO_2, H_2O and low TiO_2 contents compared to tholeiitic suites [*Crawford et al*., 1989; *Le Maitre et al*., 1989; *Le Bas*, 2000, > 52 wt% SiO_2, MgO > 8 wt% and TiO_2 < 0.5 wt%]. They lack plagioclase in rocks more mafic than andesite, and contain very magnesian olivine phenocrysts [up to Fo_{94}, *Crawford et al.,* 1989].

[19] The petrology, geochemistry and mineralogy of North Tongan high-Ca boninites have been presented in a number of previous papers [*Sharaskin et al.,* 1983; *Falloon and Green,* 1986; *Danyushevsky and Sobolev*, 1987; *Falloon et al.,* 1987, 1989; *Falloon and Crawford*, 1991; *Danyushevsky et al.,* 1992; *Sobolev and Danyushevsky*, 1994; *Danyushevsky et al.,* 1995, and references therein].

[20] Two studies using independent approaches to understanding high-Ca boninite petrogenesis [*Sobolev and Danyushevsky*, 1994; *Falloon and Danyushevsky*, 2000] both conclude that high-Ca boninite petrogenesis requires temperatures as high as ~1480°C at depths of ~45 km in the mantle wedge. These high temperatures are consistent with the model proposed by *Danyushevsky et al.* [1995] which involves melting of Samoan plume mantle [component D1 in the model of *Danyushevsky et al.,* 1995] which has moved across the 'slab window', formed by the transform fault – trench intersection, above the subducting Pacific plate, where H_2O-rich fluids, resulting from dehydration processes occurring within subducted Pacific oceanic crust [component E1 in the model of

Danyushevsky et al., 1995], fluxed the hot refractory OIB mantle generating a range of boninite melt compositions. The model of *Danyushevsky et al.* [1995] also requires a separate low-degree OIB derived silicate melt fraction as a distinct component in the petrogenesis of the high-Ca boninites [component E2 in the model of *Danyushevsky et al.,* 1995]. The new data presented in this paper combined with recent and more comprehensive data on the Samoan plume [*Workman et al.,* 2004] allows us to specifically identify the likely components in the complex heterogeneous Samoan plume involved in the high-Ca boninite petrogenesis.

4.2. Major and trace element geochemistry

[21] In Figure 5 the TiO_2 vs SiO_2 compositions of the analysed glasses (Table 4) are compared to glasses previously analysed from North Tongan boninites and the Kings Triple Junction. The range of TiO_2 and SiO_2 contents is significant and demonstrates that there is a clear association of both back-arc basin type magmas and boninites with rifting at the termination of the Tonga Trench. Below we briefly present in general terms the geochemical characteristics of the Melville dredge rocks with respect to previous sampling by pre-1996 cruises.

4.2.1 Dredge 120, 16-9/10 and KTJ lavas

[22] The geochemistry of pillow lavas recovered by Mir submersible from the KTJ have been presented by *Falloon et al.* [1992]. Pillow lavas range from basalt to andesite (Figure 5a, b), and based on geochemistry, *Falloon et al.* [1992] distinguished two groups of lavas. Type I lavas most closely resemble N-Morb in terms of major and trace element geochemistry whereas the type II lavas more closely resemble E-Morb or BABB the distinctive primary magma type identified by *Sinton and Fryer* [1987]. The type I and II designation is equivalent to the 'depleted' and 'enriched' types respectively of *Volpe et al.* [1988] for lavas dredged from the central parts of the Lau Basin, and the (N)-type and (T)-type Lau back-arc basin basalts respectively of *Hawkins and Melchior* [1985]. Type I lavas from the KTJ have very low K_2O (<0.14w%), LREE-depleted REE patterns, and similar incompatible element abundances to N-Morb, except for slightly higher Rb and Ba contents [*Falloon et al.,* 1992]. Type II lavas from the KTJ have higher K_2O (>0.14wt%), LREE-depleted to enriched REE patterns, and significant enrichments in LILE compared to N-Morb, but similar to those observed in the BABB magma type. The type II lavas have Al_2O_3 and FeO contents intermediate between trends displayed by BABB and N-Morb suites of glasses [*Falloon et al.,* 1992]. Pillow basalts recovered by D120 on the northern Lau spreading center associated with the northeastern arm of the KTJ are basaltic andesites. The major element chemistry of glasses from D120 are very similar to the type II glasses from the KTJ [*Falloon et al.,* 1992]. However the D120 glasses compared to the type II glasses from the KTJ at a given MgO content have lower TiO_2 contents (Figure 5a).

[23] The Kallisto station 16-9 and 10 lavas are similar to backarc basin lavas from the Nifonea Ridge in the Coriolis Trough, Vanuatu in terms of relatively high TiO_2 compared to typical back-arc basin basalts [Figure 5a; *McConachy et al.,* 2005]. High TiO_2

contents are normally associated with intra-plate magmatism but as *McConachy et al.* [2005] argue the Coriolis Trough lavas despite, having strong alkali enrichment, do not belong to within-plate magma type but represent a globally unique end-member of the back-arc basin magmatism associated with incipient back-arc basin rifting. *McConachy et al.* [2005] propose that the alkali and associated LREE-enrichment (Figure 6) seen in the Coriolis Trough lavas is the result of low-degree partial melting of a relatively fertile mantle source as the result of the incipient rifting behind the volcanic front. In contrast to the Coriolis Trough lavas, station 16-9 and 10 backarc pillow lavas, although having similar TiO_2 contents to the Coriolis Trough lavas, are significantly enriched in K_2O (Figure 5) and LREE (Figure 6) compared to normal backarc basin lavas, such as those from the KTJ. We thus do not think that this is pure backarc rifting. Consistent with a more complicated origin, *Zlobin et al.* [1991] considered these lavas to be ‘OIB-like’. However the lavas were clearly erupted on the back-arc side of the trench (and not accreted from the Pacific Plate) as they contain cumulate xenoliths related to boninite magmas [*Zlobin et al*., 1991].

4.2.2. Dredges 113, 115, 118 and eastern group boninites

[24] The new sampling during BMRG08MV recovered boninites which are consistent with previous sampling in this area. D113 and D115 recovered boninite lavas with U-shaped REE patterns (Figure 7) similar to boninites from Natsushima station 21. D115 occurred close to Natsushima station 23 where the most depleted boninites from the Northern Tonga area were found (samples 5-24 and 5-28, Figure 8). One of the station 23 boninites, sample 5-25, has a number of odd features which indicates that it has a more complex petrogenesis than other eastern group boninites. Melt and spinel inclusions in olivine indicate that this sample is a mixed magma (*Falloon et al.,* [1989]; *Danyushevsky et al.,* [1995]). The most magnesian olivines (Fo94) have spinel and melt inclusion compositions identical to the other depleted station 23 boninites (5-24, 5-28) however the more evolved olivines (Fo90) have melt inclusions indicating a melt with lower SiO_2 and higher FeO contents and spinels inclusions with significantly lower Al_2O_3 contents. Sample 5-25 (and associated basaltic andesites 5-20 and 5-27) has a flat REE pattern and Sr-Nd-Pb isotopic values similar to southern Tofua Arc lavas (Figures 8, 10). The chemical features of this sample may reflect interaction of high-Ca boninite melts or mantle sources with the modern Tofua Arc magmatic system. Unfortunately the small size of the sample itself precludes any detailed chemical, mineralogical and experimental study of melt inclusions, which are necessary to clarify its origin.

[25] Whole rock compositions from D118 located on a large volcanic edifice within the graben at the northern end of the Tonga Ridge (Figures 2 and 3) are rhyolite. The glass from D118 also represents a strongly silica enriched magma. As it can be seen from Figure 7 the rhyolites have very strong affinities to boninites from station 21 recovered by the Natsushima voyage. *Falloon and Crawford* [1991] demonstrated that in general the variation in the Station 21 lavas were consistent with the process of fractional crystallization. The composition of D118 represents a highly evolved magma composition derived from a parent similar to station 21 lavas. We therefore infer that the large volcanic edifice occupying the graben at the northern end of the Tonga is the result

of the boninite magmatism associated with rifting at the northern termination of the Tonga Trench.

4.2.3. Dredges 116, 117, 119 and western group boninites

[26] The boninites recovered at D119 have strongly enriched REE patterns (Figure 9) consistent with boninites recovered at station 26 and 24 and 25 of the Kallisto and Natsushima voyages. Interestingly the 'western' group boninites show a range of REE patterns including: (1) those with relatively flat MREE to HREE (16-26/2, 6-3, 119-1-1); (2) those with a slight 'U' shaped pattern (16-26/1, 119-2-5) and (3) those with a steadily increasing REE abundances from Lu to La, such as 7-18. The REE pattern for the 7-18 boninite, as noted by previous workers [*Falloon and Crawford*, 1991; *Danyushevsky et al.,* 1995) resembles that of OIB melts from the Samoan plume, such as sample 16-94/1 from the Uo Mamae seamount (Figure 9).

[27] The sampling of the large back-arc caldera (D116 and D117), as with D118, recovered evolved dacites and rhyolites which, based on their TiO_2 (Figure 5a) and REE abundance patterns (Fig.9), are derived from boninite parental magmas. The D116 and D117 lavas have remarkably similar REE patterns to the 'western group' boninites displaying relatively flat middle to heavy REE patterns.

4.3. Isotope geochemistry

[28] The Nd, Sr and Pb isotope geochemistry of samples analysed in this study are presented and compared to other relevant data sets in Figures 10-13. In general terms the isotope values of the boninites and other lavas recovered from the northern Lau Basin and the termination of the north Tonga Ridge are intermediate between MORB and OIB lavas. The significance of this general observation and the petrogenetic interpretation presented in this work builds on the results and conclusions of *Hergt and Hawkesworth* [1994] and *Workman et al.* [2004]. *Hergt and Hawkesworth* [1994] made two very important observations: (1) they showed on the basis of Nd, Sr and Pb isotopic compositions that the mantle source of Lau backarc basin lavas changed from an initial Pacific type MORB source mantle to an Indian type MORB source mantle which is presently involved in the eruption of back-arc magmas in the modern Lau Basin spreading centers such as the Central Lau Spreading Center (Figure 1) and (2) they noted that in $^{208}Pb/^{206}Pb$ vs $^{206}Pb/^{204}Pb$ lead isotope space the modern Lau Basin magmas defined an array parallel to Pacific MORB mantle and the modern Tofua arc magmas. *Workman et al.* [2004] have documented the isotopic composition and evolution of the Samoan plume in extraordinary detail, allowing for the first time a detailed examination of possible Samoan plume components involved in the north Tonga high-Ca boninite petrogenesis. Of particular significance is the observation that not all seamounts located close to the line of the Samoan plume are associated with it. In particular *Workman et al.* [2004] noted that the Malulu seamount and Rose Atoll to the east of Vailulu'u are most likely part of the Cook-Austral mantle plume [*Workham et al.,* 2004]. This observation is of significance as it allows the possibility of invoking a mantle plume component other than the Samoan plume into the petrogenesis of Tongan arc lavas. Both *Falloon et al.*

[1989] and *Falloon and Crawford* [1991] noted on the basis of Nd and Sr isotopes that a OIB component other than the Samoan plume must be involved in mantle sources of northern Tongan lavas, and that the Cook-Austral plume was the most likely extra OIB component. As an alternative to the Cook-Austral plume several subsequent workers, also recognizing the need for an additional enriched component, have proposed subducted volcaniclastic sediment from the Louisville Ridge as the cause of the enriched isotopes seen in the northern Tongan islands of Tafahi and Niuatoputapu [*Turner and Hawkesworth,* 1998, *Ewart et al.,* 1998, *Regeulous et al.,* 1997, *Wendt et al.,* 1997]. However, as discussed by *Danyushevsky et al.* (1995), the Louisville Ridge is unlikely to be involved due to its significantly lower $^{87}Sr/^{86}Sr$ ratios compared to the northern Tonga lavas (Figure 13).

[29] In Figure 10 we present new $^{208}Pb/^{204}Pb$ and $^{206}Pb/^{204}Pb$ values of our sampling during BMRG08MV and selected pre-1996 cruises (Table 6). The new data presented here confirms that two enriched mantle components are required and strongly suggests that both the Samoan and the Cook-Austral plume are the most likely sources of the enriching OIB component. As can be seen in Figure 10 all our samples, except boninitic rhyolite D116 from the large back-arc caldera, have Pb isotope compositions consistent with mixing between Indian MORB source mantle and the Samoan Plume. The samples define a general trend that parallels the lavas from the Tofua Arc and the northern islands of Tafahi and Niuatoputapu. Sample D116 has Nd, Sr and Pb isotope values identical to these two northern Tongan islands (Figures 10 and 13). The general trend of the Tofua arc volcanics is consistent with mixing between Pacific MORB source mantle and a plume component similar to the Cook-Austral Islands [*Hergt and Hawkesworth*, 1994]. The fact that the northern most Tongan islands of Tafahi and Niuatoputapu have the most enriched isotope values is consistent with the hypothesis that the Cook-Austral plume mantle has penetrated across the 'slab window' and mixed with Pacific MORB mantle, most likely during the early history of the opening of the Lau Basin when we know that Pacific MORB mantle was the source for Lau Basin spreading centers [*Hergt and Hawkesworth*, 1994].

5. Discussion

5.1. Modeling of Nd and Sr isotopes

5.1.1. Northern Lau Basin back-arc basalts

[30] In Figure 11 we present our results of modeling the Sr and Nd isotopic variation in the northern Lau Basin back-arc basalts. *Volpe et al.* [1988] demonstrated that the Sr and Nd isotopic compositions of Lau Basin basalts displayed a bimodal distribution which is related to geographic location with the Lau Basin. Volpe *et al.* [1988] defined two types of basalt comprising both N and E types; Type I basalts ($^{87}Sr/^{86}Sr \leq 0.7037$, $^{143}Nd/^{144}Nd \geq 0.51297$) occur along the Peggy ridge and seafloor to the south, and Type II basalts ($^{87}Sr/^{86}Sr \geq 0.738$, $^{143}Nd/^{144}Nd \leq 0.51288$) which have been recovered from spreading ridges and seafloor north of the Peggy Ridge.

[31] *Volpe et al.* [1988] noted that the Sr-Nd compositions of Type II lavas are similar to OIB, including recent alkali basalts from Fiji [*Gill*, 1984], and from the South Pandora Ridge in the North Fiji basin [*Sinton et al.,* 1991]. They also noted that the restriction of Type II basalts to the northeastern portion of the Lau Basin indicates that there are localised mantle domains with distinct compositions. Further work [*Loock*, 1990; *Falloon and Crawford*, 1991; *Hergt and Hawkesworth*, 1994; *Ewart et al*., 1998] subsequent to *Volpe et al.* [1988] has confirmed these observations and it is clear that the Peggy Ridge lies on the boundary between two mantle domains, Morb-like to the south (Pacific evolving to Indian) and OIB like to the north. This is also supported by $^{3}He/^{4}He$ ratios of northern Lau Basin basalts [*Poreda*, 1985; *Poreda and Craig*, 1993].

[32] *Volpe et al.* [1998] noted two trends (as shown in Figure 11) in the basalt data from the northeastern Lau Basin. Trend I parallels the MORB-OIB array and includes post subduction alkali basalts from Fiji and the Pandora ridge lavas, trend II includes lavas from the island of Niua fo'ou and is gradational between MORB and undersaturated post-erosional Samoan basalts [*Wright and White*, 1986]. The Island of Niua fo'ou in the northern Lau Basin has long been recognized as having a distinctive mantle source in terms of its isotopic values. *Ewart and Hawkesworth* [1987] noted the similarities of the isotopic compositions of Niua Fo'ou lavas and lavas from the Samoan and Cook Island chains suggesting that Niua fo'ou may be tapping a mixed asthenosphere source. *Ewart et al.* [1998] suggest that Niua fo'ou represents a separate 'mini-plume' from deeper within the Lau Basin, possibly involving mixing of the 'new' (Indian) Lau Basin MORB-source with a restricted isotopic subset of the Samoan plume arrays. The new work on the Samoan plume by *Workman et al.* [2004] has allowed a more detailed picture of the isotopic complexity of the Samoan plume source and an enhance ability to identify distinctive isotopic subsets. In Figure 11 we model the trends identified by *Volpe et al*. [1988] as mixtures between a depleted Peggy Ridge N-Morb end-member (Table 7) and OIB melt components from the Upolu Post-erosional lavas (Trend 2, Table 7) and OIB melt from the Uo Mamae seamount (Trend 1, Table 7).

[33] The data indicate that there is a generalised influence of the Samoan Plume mantle within the Lau Basin however, this influence is only reflected in the isotopic compositions of erupted lavas, but not in their major or trace element compositions which are typical for the range expected for backarc spreading centers. This observation is consistent with mixing of sources in the mantle (the Samoan mantle flowing into the northern Lau Basin through the slab window).

[34] However for D120 and 16-9/10 we clearly see an influence in major and trace elements, but still can identify them as backarc basin basalts. We speculate that this case we have a direct influence of Samoan mantle-derived melts directly into the spreading ridge (sampled by D120) and incipient rifts (sampled at 16-9/10). We have therefore modeled the trace element and isotopic compositions of the KTJ and D120 lavas as mixture between a refractory Lau Basin magma and an OIB component from the Samoan plume that we believe is more clearly identified in the station 16-9/10 pillow lavas (Figure 11).

5.1.2. Eastern and Western group boninites

[35] Previous isotopic data on high-Ca boninites has been presented by *Falloon et al.* [1989] and *Danyushevsky et al.* [1995] and our new data is consistent with this work with the exception of sample 5-24 from station 23. Sample 5-24 is the most depleted boninite sample in terms of REE and HFSE, and was considered by *Danyushevsky et al.* [1995] to be close to the depleted component end-member (D1) required in the petrogenesis of the boninites (see Figure 12). The depleted component D1 was considered to be refractory OIB mantle (Samoan plume) on the basis of (1) low $^{143}Nd/^{144}Nd$ isotopes in sample 5-24 [0.51277, *Falloon et al*., 1989] within the range of Samoan OIB and (2) very high temperatures established for the primary melt for this depleted component (~1480°C at ~45km) confirmed by two independent experimental studies [*Sobolev and Danyushevsky*, 1994; *Falloon and Danyushevsky*, 2000]. In our new work we have reanalysed sample 5-24 (3 repeat separate dissolutions, Table 6) and have obtained an average $^{143}Nd/^{144}Nd$ value of 0.512973 significantly higher than previously analysed. To confirm our new result we also analysed sample 5-28, a depleted boninite like 5-24, which has a $^{143}Nd/^{144}Nd$ value of 0.512959. In the model of *Danyushevsky et al*. [1995] the depleted boninites are formed by the fluxing of a refractory Samoan mantle (D1) by a subduction-related H_2O fluid (E1) enriched in LILE. That model assumed that the middle REE were not transported by the slab-derived fluid as this fluid (which should have Nd of the subducted Pacific ocean crust with >0.5129) appeared not to change the isotopic composition of the mantle Nd. However recent experimental work on likely subduction zone fluid compositions [*Kessel et al*., 2005] demonstrate that middle-REE are fluid mobile. The new values obtained for 5-24 are thus more consistent with the model of *Danyushevsky et al*. [1995] because the subduction zone fluid will impose its isotopic value onto a refractory source.

[36] Our new results strongly suggest that the depleted hot refractory OIB mantle component $^{87}Sr/^{86}Sr$ and $^{143}Nd/^{144}Nd$ values reflect those of a slab-derived fluid which has overprinted the original OIB residue. This scenario is in hindsight more consistent with the model of *Danyushevsky et al*. [1995], as the refractory OIB mantle component [D1 of *Danyushevsky et al*., 1995] has a strong slab-derived enrichment in LILE and H_2O, reflected in high LILE/HFSE values and high H_2O/K_2O, H_2O/Al_2O_3, and H_2O/Na_2O values in olivine-hosted melt inclusions [*Danyushevsky et al*. 1995]. In Figure 12 we show the results of our modeling of the $^{87}Sr/^{86}Sr$ and $^{143}Nd/^{144}Nd$ values of the Western and Eastern group boninites. Three components labeled D1, E1 and E2 on Figure 12 are required: D1 is the refractory OIB mantle residue from the Samoan plume. The hottest part of the plume should be reflected in the main shield building lavas from Upolu; E1 is a slab-derived H_2O rich fluid carrying LILE and light-middle REE. We have modeled the composition of this fluid by assuming that all the H_2O, Sr and Nd present in the depleted boninites is derived from the slab-fluid. In this case the fluid composition has an isotopic composition identical to sample 5-24, and the fluid has a calculated abundance of Sr and Nd of 2380 and 40ppm respectively (Table 7). The isotopic values are consistent with the fluid being derived from Pacific ocean crust, which has experienced seafloor alteration (as indicated on Figure 12); E2 which has a high $(La/Yb)_N$~16 is an incompatible element-enriched silicate melt derived from the Samoan

plume OIB source. This is the main enriching component seen in the north Tongan boninites and completely obscures the influence of the slab-derived fluid on the geochemistry of the enriched boninites [*Danyushevsky et al.,* 1995]. In our modeling we have chosen the backarc rift related pillow lava from station 16-10/4 as representative of the enriched component from the Samoan plume (the values of this end-member are also given in Table 7). As can be seen from Figure 12 the mixing between a depleted boninites represented by 5-24 and 5-28 and the 16-10/4 composition can successfully explain the isotopic and trace-element abundances (see [40]) in the Western and Eastern group boninites (Figure 12 and see also Figure 14 and 15). Also shown in Figure 12 for comparison is a mixing line between 5-24 and an OIB melt from Uo Mamae (orange dotted line, Figure 12).

5.1.3. Back-arc caldera (D116) and Tofua Arc volcanics

[37] The isotopic composition of the large back-arc caldera sampled by D116 and D117 (Figures 2 and 3) is unique in that it is the only volcanic feature that has been sampled behind the arc that has erupted lavas that have the same $^{208}Pb/^{206}Pb$ as the northern Tofua Arc islands of Tafahi and Niuatoputapu (Figures 10 and 13). As discussed above we believe that the relatively enriched Sr and Nd isotopic values of the northern Tofua Arc islands require a different plume component other than the Samoan Plume (cf. *Turner et al.,* 1997; *Regeulous et al*., 1997; Wendt *et al*., 1997; *Ewart et al*., 1998]. In Figure 13 we can successfully model the Sr and Nd isotopic values of D116-1-3 by mixing between a depleted Pacific Morb end-member represented by ODP hole 834 and an OIB mantle component from the Cook-Austral Islands (Table 7). The Cook-Austral Islands and associated seamounts are assumed to have been formed by the same hotspot volcanism currently located on the MacDonald Seamount (~29°S, ~140°W) in the South Pacific [*Jordahl et al.,* 2004; *Bideau and Hekinian*, 2004]. The Cook-Austral chain which although in general conform to an absolute plate motion relative to the hot spot reference frame [*Duncan and Clague*, 1986] has a complex age progression [*Jordahl et al*., 2004] making it unlikely that a single hotspot could explain the entire chain. The oldest parts of the Cook-Austral chain (20-25Ma) however overlap the positions of seamounts and islands formed by the Samoan hotspot [*Norton*, 2000], which is currently located at the active submarine Vailulu'u volcano at ~14°S ~169°W (*Hart et al.,* 2000). We believe that mantle sources for the Tofua arc is conceivably the result of mixing between Pacific type Morb and a Cook-Austral plume component, which presumably also penetrated into the northern Lau basin. This implies that the bend in the northern Tongan trench and associated change to transform boundary may have been a stable feature for quite some time.

5.2. The model of Danyushevsky *et al.* [1995] revisited

[38] In Figures 14 and 15 we present primitive mantle normalised abundance patterns of the selected compositions from our study area. The model of *Danyushevsky et al*. [1995], as previously discussed, involves three components, a refractory mantle component (D1) and two enriching components (E1 and E2). D1 is a residual mantle derived from the Samoan plume penetrating into the northern Lau Basin across the slab window. E1 is a

slab-derived fluid and it is a pervasive presence in all volcanics from our study area. However it is only clearly seen in the lavas derived from the refractory mantle components (D1) such as sample 5-24 (Figure 14). E2 is an OIB melt component enriched in incompatible elements, also derived from presumably less refractory parts of the Samoan plume source. As can be seen from Figure 15, the enriched boninite normalised patterns show systematic changes with increasing $(La)_N$ which is consistent with increasing amounts of the enriched E2 component. In Figure 16 we present the normalised abundance patterns of new spreading center sampled at D120. As can be seen from Figure 16 the normalised pattern of D120 pillow lavas is satisfactorily explained by mixing between a depleted backarc mantle component (represented by 123 95-1) and an enriched OIB component (represented by pillow lavas Kallisto station 16-10/9).

[39] The model of *Danyushevsky et al.* [1995] invoking the melting of residual Samoan mantle was developed to explain two critical observations concerning the Tongan boninites: (1) very high temperatures (~1480°C) of the incompatible element-depleted mantle source above the subducted slab, and (2) the striking similarity between relative concentrations of incompatible elements in the most incompatible element-enriched Tongan boninite, and adjacent OIB-like lavas (Figures 14 and 15). The transition from subduction to transform tectonics in the north Tonga region forms a “window” from the mantle wedge towards the sub-Pacific mantle. *Danyushevsky et al*. [1995] suggest that this “window” is used by the Samoan Plume to penetrate the mantle wedge above the subducted slab. The eastward “rollback” of the Tonga Trench [*Carlson and Media*, 1984] created an extensional tectonic regime in the Northern Lau Basin, clearly seen in the new seafloor mapping (Figures 2 and 3). This extensional regime has caused part of the Samoan plume to drawn into the mantle wedge above the slab. The gradual eastward shift of the rigid subducted lithosphere is likely to result in the removal of the outer colder parts of the Samoan plume exposing the hotter inner parts above the slab. Once above the slab, and having been depleted during previous formation of OIB melts, hot residual plume lherzolite (component D1) interacts immediately with H_2O-rich fluids derived from the subducted slab (component E1), producing primary high-Ca boninite melts. *Danyushevsky et al.* (1995) suggested two possible scenarios of mixing between primary high-Ca boninite melts produced during melting of component D1, and the E2 component. The first is that this mixing occurs en route to the surface, during which different batches of primary high-Ca boninite melts mix in different proportions with earlier- or simultaneously-formed OIB melts (component E2), to produce the observed chemical spectra of high-Ca boninites (Figures 14 and 15). This mechanism assumes that boninites and OIB melts were formed from different parts of the plume. The second possibility is that actual mixing took part in the mantle during boninite primary melt genesis. In this case the E2 component represents residual melts which have not separated from their sources during OIB magma genesis. At the present time it is not possible to distinguish between these two possibilities, however the presence of back-arc basalts from Kallisto stations 16-10/9 which have a strong Samoan plume signature supports the first of these scenarios.

5.3. Tectonic implications

[40] If we are correct in our hypothesis that the ‘slab-window’ has been a relatively long-lived tectonic feature of this area then we would predict that boninites with a strong Cook-Austral plume geochemical signature (especially Pb isotopic values) should be present either at deeper stratigraphic levels in the landward slope of the Trench wall, or alternatively located in older rift basins further to the west, which have been moved there as a consequence of Lau Basin opening.

[41] As back-arc spreading developed in the Lau Basin, we had a change in mantle source from Pacific to Indian [*Hergt and Hawkesworth*, 1994] and we infer that the movement of the Samoan plume across the slab window was coincident with this change, as all the northern Lau back-arc basin lavas, such as from the KTJ and sampled at D120 appear to be a mixture between Indian Morb mantle and Samoan plume mantle in $^{208}Pb/^{206}Pb$ and $^{206}Pb/^{204}Pb$ isotopic space (Figure 10).

6. Conclusions

[42] (1) New seabeam mapping [*Wright et al.,* 2000] reveals that the boninites erupted at the northern termination of the Tonga Trench and sampled by R/V Kallisto, Natsushima and Melville are clearly related to recent rifting along the trench-transform wall. The boninite dredge locations are derived either from young volcanic cones associated with rift grabens or recovered from the rifted walls of a prominent graben which cuts the North Tonga Ridge at its northern terminus.

[43] (2) Our new results confirm the earlier work of *Danyushevsky et al.* [1995] that hot residual mantle from the Samoan plume penetrating across the ‘slab-window’ into the mantle wedge is the primary cause for high-Ca boninite magmatism at the northern termination of the Tonga Trench.

[44] (3) Back-arc pillow lavas recovered from the northern most nascent spreading center in the northern Lau Basin at D120 are BABB-like basaltic andesites with LREE enriched patterns and Sr, Nd isotope values consistent with mixing with an OIB melt component from the Samoan Plume. Our results support models that demonstrate that the northern Lau Basin mantle source is a hybrid between Indian MORB source mantle and the Samoan Plume mantle [*Volpe et al*., 1988; *Ewart et al*., 1998].

[45] (4) Volcanics recovered from a large back-arc caldera (D116 and 117) have Sr, Nd and Pb isotopic values similar to the northern Tofua Arc islands of Tafahi and Niuatoputapu. We argue that the isotopic composition of the caldera volcanics and the northern most Tofua Arc lavas are consistent with the model of mixing between Pacific Morb mantle and a component from the Cook-Austral plume. We propose that the ‘slab window’ may have been a relatively long-lived stable tectonic feature, allowing Pacific Morb mantle and Cook-Austral plume mantle to mix possibly at an early stage in the history of the Lau Basin opening. If the current ‘slab-window’ is a long lived tectonic feature we would predicts the existence of older boninites (>10Ma), located at deeper stratigraphic levels in the northern Lau Basin-Tonga ridge crust or alternatively located in older rift grabens further to the west along the transform fault boundary, which were the

result of interaction between hot residual Cook-Austral plume source mantle and subduction-related fluids. Further sampling in this area is therefore necessary to test this model.

Acknowledgements

[46] This research was supported by the Australian Research Council and by NSF grants OCE-9521023 and OCE-9521039. We wish to thank all the scientists, officers, and crew who participated in all the cruises mentioned. We acknowledge support of the Museum of Natural History, Washington, DC, which provided electron microprobe standards.

References

Acland, A. S. (1996), Magma genesis in the northern Lau Basin, S. W. Pacific. Unpublished Ph.D thesis, University of Durham. 260pp.

Bevis, M., F. W. Taylor, B. E. Schultz, J. Recy, B. L. Isacks, S. Helu, R. Singh, E. Kendrick, J. Stowell, B. Taylor, and S. Calmant (1995), Geodetic Observations of Very Rapid Convergence and Back-arc Extension at the Tonga Arc, *Nature, 374*, 249-251.

Bideau, D., and R. Hekinian (2004), Intraplate gabbroic rock debris ejected from the magma chamber of the Macdonald Seamount (Austral hotspot): Comparison with other provinces, in *Oceanic Hotspots: intraplate submarine magmatism and tectonism*, edited by R. Hekinian, P. Stoffers, and J. L. Cheminee, pp. 309-348, Springer-verlag, Berlin.

Bloomer, S.H., D. Wright, C. J., MacLeod, D. Tappin, P. Clift, T. J. Falloon, R. L. Fisher, K. Gillis, T. Ishii, M. Kelman, K. Mafi, H. Sato, and M. Winowitch (1996), Geology of the Tonga Forearc: A Supra-Subduction Zone Ophiolite.*Transactions American Geophysical Union, Fall meeting, San Francisco, 77 (46)*, p.325.

Carlson, R. L., and P. J. Melia (1984), Subduction hinge migration, *Tectonophysics, 102*, 399-411.

Chen, Q., K. –H. Park, J. D. Macdougall, A. Zindler, G. W. Lugmair, H. Staudigel, J. Hawkins, and P. Lonsdale (1987), Isotopic evidence for a hotspot origin of the Louisville Seamount Chain, *American Geophysical Union Geophysical Monograph, 43,* 283-296.

Crawford, A. J., T. J. Falloon, and D. H. Green (1989), Classification, petrogenesis and tectonic setting of boninites, in *Boninites and Related Rocks*, edited by A. J. Crawford, pp. 1-49, Unwin and Hyman, London.

Danyushevsky, L. V., and A. V. Sobolev (1987), New data on the petrology of boninites in Tonga, *Geol., Geophys., 12*, 100-103 (in Russian).

Danyushevsky, L. V., A. V. Sobolev, and N. N. Kononkova (1992), Methods of studying magma inclusions in minerals during investigations on water-bearing primitive mantle melts (Tonga trench boninites), *Geochemistry International, 29*, 48-62.

Danyushevsky, L. V., A. V. Sobolev, and T. J. Falloon (1995), North Tongan high-Ca boninite petrogenesis: The role of Samoan plume and subduction zone-transform fault transition. *Journal of Geodynamics 20*, 219-241.

Duncan, R. A., and D. A. Clague (1986), Pacific plate motion recorded by linear volcanic chains, in *The Pacific Ocean, The Ocean Basins and Margins*, vol.7A, edited by A. E. M. Nairn, F. G. Stehli, and S. Uyeda, pp.89-121, Plenum, New York.

Eggins S. M., J. D. Woodhead, L. P. J. Kingsley, G. E. Mortimer, P. Sylvester, M. T. McCulloch, J. M. Hergt, and M. R. Handler (1997). A simple method for the precise determination of ≥40 trace elements in geological samples by ICPMS using enriched isotope internal standardisation. *Chemical Geology, 134*, 311-326.

Ewart, A., and C. J. Hawkesworth, (1987), The Pleistocene-Recent Tonga-Kermadec arc lavas: interpretation of new isotopic and rare earth data in terms of a depleted mantle source model. *J. Perol., 28*, 495-530.

Ewart, A., W. B. Bryan, B. W. Chappell, R. L. Rudnick (1994), Regional Geochemistry of the Lau-Tonga Arc and Back-arc systems, in *Proceedings of the Ocean Drilling Program, Scientific Results 135*, edited by J. Hawkins, L. Parson, J. Allen, et al., pp. 385-425, Ocean Drilling Program, College Station, Texas.

Ewart, A., K. D. Collerson, M. Regelous, J. I. Wendt, and Y. Niu (1998), Geochemical evolution within the Tonga-Kermedec-Lau Arc-Back-arc systems: The role of varying mantle wedge composition in space and time, *J. Petrol., 39*, 331-368.

Falloon, T. J., and D. H. Green (1986), Glass inclusions in magnesian olivine phenocrysts from Tonga: evidence for highly refractory parental magmas in the Tongan arc, *Earth and Planetary Science Letters, 81*, 95-103.

Falloon, T. J., and A. J. Crawford (1991), The petrogenesis of high-calcium boninite lavas dredged from the northern Tonga ridge, *Earth and Planetary Science Letters, 102*, 375-394.

Falloon, T. J., and L. V. Danyushevsky (2000), Melting of Refractory Mantle at 1.5, 2 and 2.5 Gpa under Anhydrous and H2O-undersaturated Conditions: Implications for the Petrogenesis of High-Ca Boninites and the Influence of Subduction Components on Mantle Melting, *Journal of Petrology, 41*, 257-283.

Falloon, T. J., D. H. Green, and A. J. Crawford, (1987), Dredged igneous rocks from the northern termination of the Tofua magmatic arc, Tonga and adjacent Lau Basin. *Australian Journal of Earth Sciences, 34*, 487-506.

Falloon, T. J., D. H. Green, and A. J. Crawford (1989), Petrogenesis of high-Mg and associated lavas from the north Tonga trench, in *Boninites and Related Rocks*, edited by A. J. Crawford, pp. 357-395, Unwin Hyman, London.

Falloon, T.J., S. H. Bloomer, and A. J. Crawford (1997), Boninites recovered from the Tonga Forearc. EOS, *Transactions American Geophysical Union, Fall meeting, San Francisco, 78 no.46*, p.815.

Falloon, T. J., A. Malahoff, L. P. Zonenshain, and Y. Bogdanov (1992), Petrology and geochemistry of back-arc basin basalt from Lau Basin spreading ridges at 15°, 18° and 19° S. *Mineralogy and Petrology, 47*, 1-35.

Falloon, T. J., D. H. Green, A. L. Jaques, and J. W. Hawkins (1999), Refractory magmas in back-arc basin settings – experimental constraints on the petrogenesis of a Lau Basin example, *J. Petrol., 40*, 255-277.

Gill, J. B. (1976), Composition and age of Lau Basin and Ridge volcanics: implications for evolution of an interarc basin and remnant arc, *Geological Society of America Bulletin, 87*, 1384-1395.

Gill, J. B. (1984), Sr-Pb-Nd isotopic evidence that both MORB and OIB sources contribute to oceanic island arc magmas in Fiji. *Earth and Planetary Science Letters, 68*, 443-458.

Govers, R., and M. J. R. Wortel (2005), Lithosphere tearing at STEPS faults: response to edges of subduction zones. *Earth and Planetary Science Letters, 236*, 505-523.

Hart, S. R., H. Staudigel, H., A. A. P. Koppers, J. Blusztajn, E. T. Baker, R. Workman, M. Jackson, E. Hauri, M. Kurz, K. Sims, D. Fornari, A. Saal, and S. Lyons (2000), Vailulu'u undersea volcano: The New Samoa, *Geochem. Geophys. Geosyst., 1*, Paper number 2000GC000108.

Hawkins, J. W., and J. T. Melchior (1985), Petrology of Mariana Trough and Lau Basin basalts. *J. Geophys. Res., 90*, 11431-11468.

Hergt, J. M., and C. J. Hawkesworth (1994), Pb-, Sr-, and Nd-isotopic evolution of the Lau Basin: implications for mantle dynamics during back-arc opening, in *Proceedings of the Ocean Drilling Program, Scientific Results 135*, edited by J. Hawkins, L. Parson, J. Allen, et al., pp. 505-517, Ocean Drilling Program, College Station, Texas.

Jarosewich, E. J., J. A. Nelen, and J. A. Norberg (1980), Reference samples for electron microprobe analyses, *Geostandards Newsletter, 4*, 257-258.

Jordahl, K. A., M. K. McNutt, and D. W. Caress (2004), Multiple episodes of volcanism in the Southern Austral Islands: Flexural constraints from bathymetry, seismic reflection, and gravity data, *J. Geophys. Res., 109*, B06103, doi:10.1029/2003JB002885.

Kamenetsky, V. D., and R. Maas (2002), Mantle-melt evolution (dynamic source) in the origin of a single MORB suite: a perspective from magnesian glasses of Macquarie Island, *Journal of Petrology, 43*, 1909-1922.

Kessel, R., M. W. Schmidt, P. Ulmer, and T. Pettke (2005), Trace element signature of subduction-zone fluids, melts and supercritical liquids at 120-180km depth, *Nature, 437*, 724-727.

Le Bas, M. J. (2000), IUGS Reclassification of the High-Mg and Picritic Volcanic Rocks, *Journal of Petrology, 41*, 1467-1470.

Le Maitre, R. W., P. Bateman, A. Dudek, J. Keller, J. Lameyre, M. J. Le Bas, P. A. Sabine, R. Schmid, H. Sorensen, A. Streckeisen, A. R. Woolley, and B. Zanettin (1989), *A Classification of Igneous Rocks and Glossary of Terms: Recommendations of the International Union of Geological Sciences Subcommission on the Systematics of Igneous Rocks*, Oxford, Blackwell Scientific, 193pp.

Loock, G., W. F. McDonough, S. L. Goldstein, A. W. Hofmann (1990), Isotopic compositions of volcanic glasses from the Lau Basin, *Marine Mining, 9*, 235-245.

MacLeod, C. J. (1996), Geodynamics of the Tonga subduction zone and Lau Backarc basins, *EOS Trans., AGU, 77*, F325

McConachy, T. F., R. J. Arculus, C. J. Yeats, R. A. Binns, F. J. A. Barriga, B. I. A. McInnes, S. Sestak, B. Rakau, and T. Tevi (2005), New hydrothermal activity and alkalic volcanism in the backarc Coriolis Troughs, Vanuatu, *Geology, 33*, 61-64.

Millen, D. W., and M. W. Hamburger (1998), Seismological evidence for tearing of the Pacific Plate at the northern termination of the Tonga subduction zone, *Geology, 26*, 659-662.

Norton, I. O. (2000), Global hotpsot reference frames and plate motion, in *The History and Dynamics of Global Plate Motions*, Geophys. Monogr. Ser., vol.121, edited by M.

A. Richards, R. G. Gordon, and R. D. van de Hilst, pp. 339-357, AGU, Washington, D. C.

Parson, L. M., and D. L. Tiffin (1993), Northern Lau Basin: backarc extension at the leading edge of the Indo-Australian plate, *Geo-Marine Lett., 13*, 107-115.

Poreda, R. (1985), Helium-3 and deuterium in backarc basin basalts: Lau Basin and Mariana Trough, *Earth and Planetary Science Letters, 76*, 244-254.

Poreda, R., and H. Craig (1993), He and Sr isotopes in the Lau Basin mantle: Depleted and primitive mantle components, *Earth Planet., Sci., Lett., 119*, 319-329.

Regeulous, M., K. D. Collerson, A. Ewart, and J. I. Wendt (1997), Trace element transport rates in subduction zones: evidence from Th, Sr and Pb isotope data for Tonga-Kermadec Lavas, *Earth and Planetary Science Letters, 150*, 291-302.

Robinson, P. (2003), XRF analysis of flux-fused discs, Geoanalysis 2003, *The 5th International Conference on the Analysis of Geological and Environmental Materials, Abstracts*, 90.

Robinson, P., A. T. Townsend, Z. Yu, and C. Munker (1999), Determination of Scandium, Yttrium and Rare Earth Elements in rocks by high resolution inductively coupled plasma-mass spectrometry, *Geostandards Newsletter, 23*, 31-46.

Sharaskin, A. Ya., I. K. Pustchin, S. K. Zlobin, and G. M. Kolesov (1983), Two ophiolite sequences from the basement of the northern Tonga arc, *Ofioliti 8*, 411-430.

Sinton, J. M., and P. Fryer (1987), Mariana Trough lavas from 18°N: implications for the origin of back arc basin basalts, *J. Geophys. Res., 92*, 12782-12802.

Sinton, J. M., R. C. Price, K. T. Johnson, H. Staudigel, and A. Zindler (1991), Petrology and geochemistry of submarine lavas from the Lau and North Fiji backarc basins in *Basin Formation, Ridge Crest Processes and Metallogenesis in the North Fiji Basin*, edited by L. W. Kroenke, and J. V. Eades, pp. 155-177, Circum-Pacific Council for Energy and Mineral Resources, Earth Science Series, vol.12, American Association Petroluem Geologists, Tulsa, Oklahoma.

Smith, G.P., D. A. Wiens, K. M. Fischer, L. M. Dorman, S. C. Webb, and J. A. Hildebrand (2001), A complex pattern of mantle flow in the Lau backarc, *Science 292*, 713-716.

Smith, W. H. F., and D. T. Sandwell (1997), Global sea floor topography from satellite altimetry and ship depth soundings, *Science. 277*, 1956-1962.

Sobolev, A. V., and L. V. Danyushevsky (1994), Petrology and Geochemistry of Boninites from the North Termination of the Tonga Trench: Constraints on the Generation Conditions of Primary High-Ca Boninite Magmas, *J. Petrol., 35*, 1183-1211.

Sun, S. –s., and W. F. McDonough (1989), Chemical and isotopic systematics of oceanic basalts: implications for mantle composition and processes, in *Magmatism in the Ocean Basins*, edited by A. D. Saunders, and M. J. Norry, pp. 313-345, Geological Society Special Publication, no. 42, London.

Tappin, D. R. (1994), The Tonga Frontal-arc basin, in *South Pacific Sedimentary Basins*, edited by P. F. Balance, pp.157-176, Elsevier, Amsterdam.

Tappin, D. R., T. R. Bruns, and E. L. Geist (1994), Rifting of the Tonga/Lau Ridge and Formation of the Lau backarc basin: evidence from site 840 on the Tonga Ridge, in *Proceedings of the Ocean Drilling Program, Scientific Results 135*, edited by J.

Hawkins, L. Parson, J. Allen, et al., pp. 367-372, Ocean Drilling Program, College Station, Texas.
Turner, S., and C. Hawkesworth (1998), Using geochemistry to map mantle flow beneath the Lau Basin, *Geology, 26*, 1019-1022.
Turner, S. P., C. J. Hawkesworth, N. W. Rogers, J. Bartlett, T. J. Worthington, J. M. Hergt, J. A. Pearce, I. E. M. Smith (1997), ^{238}U-^{230}Th disequilibria magma petrogenesis and flux rates beneath the depleted Tonga-Kermadec island arc, *Geochem., Cosmochim., Acta, 61*, 4855-4884.
Volpe, A. M., J. D. Macdougall, and J. W. Hawkins (1988), Lau Basin basalts (LBB): trace element and Sr-Nd isotopic evidence for heterogeneity in backarc basin mantle, *Earth Planet. Sci. Lett., 90*, 174-186.
Wendt, J. I., Regelous, M., Collerson, K. D., and A. Ewart (1997), Evidence for a contribution from two mantle plumes to island-arc lavas from northern Tonga, *Geology, 25*, 611-614.
Wright, D. J., S. H. Bloomer, C. J. MacLeod, B. Taylor, and A. M. Goodlife (2000), Bathymetry of the Tonga Trench and Forearc: a map series, *Marine Geophysical Researches, 21*, 489-511.
Wright, E., and W. M. White, (1986), The origin of Samoa: new evidence from Sr, Nd, and Pb isotopes, *Earth and Planetary Science Letters, 81*, 151-162.
Woodhead, J. (2002), A simple method for obtaining highly accurate Pb isotope data by MC-ICP-MS, *Journal of Analytical Atomic Spectrometry, 17,* 1381-1385.
Workman, R. K., S. R. Hart, M. Jackson, M. Regelous, K. A. Farley, J. Blusztajin, M. Kurz, and H. Staudigel (2004), Recycled metasomatized lithosphere as the origin of the enriched mantle II (EM2) end-member: Evidence from the Samoan Volcanic Chain, *Geochemistry Geophysics Geosystems, 5*, doci:10.1029/2003GC000623.
Yu Z., P. Robinson, A. T. Townsend, C. Munker, and A. J. Crawford (2000), Determination of HFSE, Rb, Sr, Mo, Sb, Cs, Tl and Bi at ng g-1 levels in geological reference materials by magnetic sector ICP-MS after HF/HCLO4 high pressure digestion, *Geostandards Newsletter, 24*, 39-50.
Zellmer, K. E., and B. Taylor (2001), A three-plate kinematic model for Lau Basin opening, *Geochemistry Geophysics Geosystems, 2*, paper number 2000GC000106.
Zlobin, S. K., G. M. Kolesov, and N. N. Kononkova (1991), Development of within-plate magmatism on the landward and offshore slopes of the Tonga Trench, *Ofioliti, 16*, 17-35.

Figure Captions

Figure 1

Schematic locality map of the Lau – Tonga supra-subduction zone, showing the regional setting of the north Tongan submarine volcanic localities. Tectonic interpretation is based on the work of *Zellmer and Taylor* [2001]. The shaded rectangles delineate the areas covered by Figures 2 to 4. Orange line is a 1500 meter bathymetric contour which outlines the Lau and Tonga Ridges and surrounds the islands (solid black) in the region. Plate boundaries (purple for spreading ridges, blue for fracture zones) are labeled as follows: CLSC, Central Lau Spreading Center; ELSC, East Lau Spreading Center; FRSC, Fonualei Rift and Spreading Center; FSC, Futuna Spreading Center; LETZ, Lau Extensional Transform Zone; PR, Peggy Ridge Transform Fault; KTJ, Kings Triple Junction; NWLSC, Northwest Lau Spreading Center. The three plates outlined by *Zellmer and Taylor* [2001] for this area are labeled: A, Australian Plate; T, Tongan Plate; N, Niuafo'ou Plate. Large bold green arrows are GPS velocities of Tonga relative to Australia, from *Zellmer and Taylor* [2001] (number next to arrows is rate in mm/yr).

Figure 2

Shaded relief bathymetric map, created from a 200 meter Sea Beam 2000 grid (Boomerang 8, *Wright et al.,* [2000]) of the northern termination of the Tonga Trench and northern Lau Basin. Seabeam bathymetry has been combined with the satellite bathymetry of *Smith and Sandwell* [1997]. Map projection is Mercator. Dredge and dive localities are indicated as follows: yellow squares, R/V Kallisto, 1982; white squares, R/V Natsushima, 1984; blue squares, R/V Keldysh/Mir 1990; and red squares, R/V Melville 1996.

Figure 3

As for Figure 2. Figure 3 shows in more detail the locations of previous dredges in this area.

Figure 4

3D relief map of the area shown in Figure 3, looking directly North. The relief is shaded from the NE. The large volcanic edifice occupying the graben structure at the northern termination of the Tonga Ridge can be clearly seen. Also clearly seen is the large backarc caldera and young volcanic cones associated with incipient rifting in this area.

Figure 5

The TiO_2 a) and K_2O b) contents versus SiO_2 for volcanic glasses recovered from the north termination of the Tonga Trench and northern Lau Basin. See text for discussion. Data sources are as follows: Samoan Plume, *Workman et al.* [2004]; Coriolis Trough, *McConachy et al*. [2005]; KTJ, *Falloon et al.* [1992]; Niua fo'ou, *Ewart et al.* [1994], *Turner et al.* [1977]; North Tongan Boninites, *Falloon et al.* [1989], *Falloon and Crawford* [1991], *Sobolev and Danyushevsky* [1994].

Figure 6

REE contents in Northern Lau Basin backarc volcanics. Data sources as follows: Coriolis Trough from *McConachy et al.* [2005], Peggy Ridge sample 123 95-1 from *Gill* [1976]. Chondrite normalizing values from *Sun & McDonough* [1989].

Figure 7

REE contents in Tongan high-Ca 'eastern group' boninites from Natsushima station 21 and Melville dredges 113, 115 and 118.

Figure 8

REE contents in Tongan high-Ca boninites from Natsushima station 23 compared to REE contents of island arc tholeiites from the island of Tafahi and southern islands of the Tofua Arc. Tafahi data from *Turner et al.* [1997], *Ewart et al.* [1998], *Wendt et al.* [1997], *Ewart et al.* [1994] and P. Robinson unpublished data; Tofua Island data from the georoc reference database (http://georoc.mpch-mainz.gwdg.de/georoc/).

Figure 9

REE contents in Tongan high-Ca 'western group' boninites from Natsushima station 24-25, Kallisto station 26 and Melville dredges 116, 117 and 119.

Figure 10

The $^{208}Pb/^{204}Pb$ isotopic compositions of submarine volcanics from the northern termination of the Tonga Trench compared to the isotopic compositions of Morb, Samoan and Cook-Austral plumes and volcanics from both the Tongan Arc and Lau Basin. Samoan data from *Workman et al.* [2004], other data sources from the georoc reference database (http://georoc.mpch-mainz.gwdg.de/georoc/). See text for discussion [28].

Figure 11

Nd and Sr isotope compositions of backarc basin volcanics from the northern Lau Basin. Arrows and dotted lines refer to modeling of mixing processes between end-member compositions presented in Table 7, see text for further discussion [32 and 37]. Data sources as for Figure 11 and the georoc database.

Figure 12

Nd and Sr isotope compositions of Eastern and Western group high-Ca boninites. Arrows refer to modeling of mixing processes between end-member compositions presented in Table 7, see text for further discussion [31]. Samoan data from *Workman et al.* [1994] and *Acland* [1996]; Pacific Morb data from georoc.

<u>Figure 13</u>

Nd and Sr isotope composition of the backarc submarine caldera sampled by D116 and volcanics from Tonga-Lau Basin. Blue line refers to modeling of mixing processes between end-member compositions presented in Table 7, see text for further discussion [39]. Data for the Louisville Ridge seamounts from *Chen et al.* [1987]. Other data sources as for Figure 11 and the georoc database.

<u>Figure 14</u>

Primitive mantle normalised trace element abundance patterns for depleted high-Ca boninite 5-24 from northern Tonga compared to adjacent pillow lava from the western most rift sampled by Kallisto at stations 9 and 10 (16-10/4). D1, E1, E2 refer to the independent petrogenetic components in the model of *Danyushevsky et al.* [1995], see text for discussion [40]. Primitive mantle normalising values from *Sun and McDonough* [1984].

<u>Figure 15</u>

Primitive mantle normalised trace element abundance patterns for enriched eastern and western group high-Ca boninites from northern Tonga. Blue and green lines are abundance patterns transferred from Figure 14 for comparison. See text for discussion [40].

<u>Figure 16</u>

Primitive mantle normalised trace element abundance patterns for representative northern Lau Basin backarc basin basalts. Blue and green lines are abundance patterns transferred from Figure 14 for comparison. See text for discussion [40].

Table Captions

<u>Table 2</u>

OSU, Oregon State University, R. Duncan analyst. UCSC, University of California Santa Cruz, J.B.Gill pers com.

<u>Table 3</u>

FeO*, refers to total iron calculated as FeO. LOI, refers to Loss on ignition. †Total, refers to original analysis sum, major elements have been resumed to 100% anhydrous in Table 3.

Table 4

Major elements have been resummed to 100% anhydrous in Table 4.

Table 5

ANU, Australian National University; UTAS, University of Tasmania; BRIS, University of Bristol. REE data is presented for sample 11-3, a Lau Basin backarc basalt from the Peggy Ridge, recovered by the Natsushima 84 cruise. REE for this sample was incorrectly reported as chondrite normalised values by *Falloon et al.* [1987, 1989]. The correct values in ppm are provided in Table 3.

Table 6

MELB, University of Melbourne; ANU, Australian National University; ADEL, University of Adelaide. For the Melbourne analyses, Sr isotopes were adjusted to SRM987 = 0.710230, Nd isotope data adjusted to LaJolla=0.511860, internal precisions (2se) ≤±0.000010. Pb isotope mass bias corrected using Tl-doping (Woodhead, 2002)

Figure 1

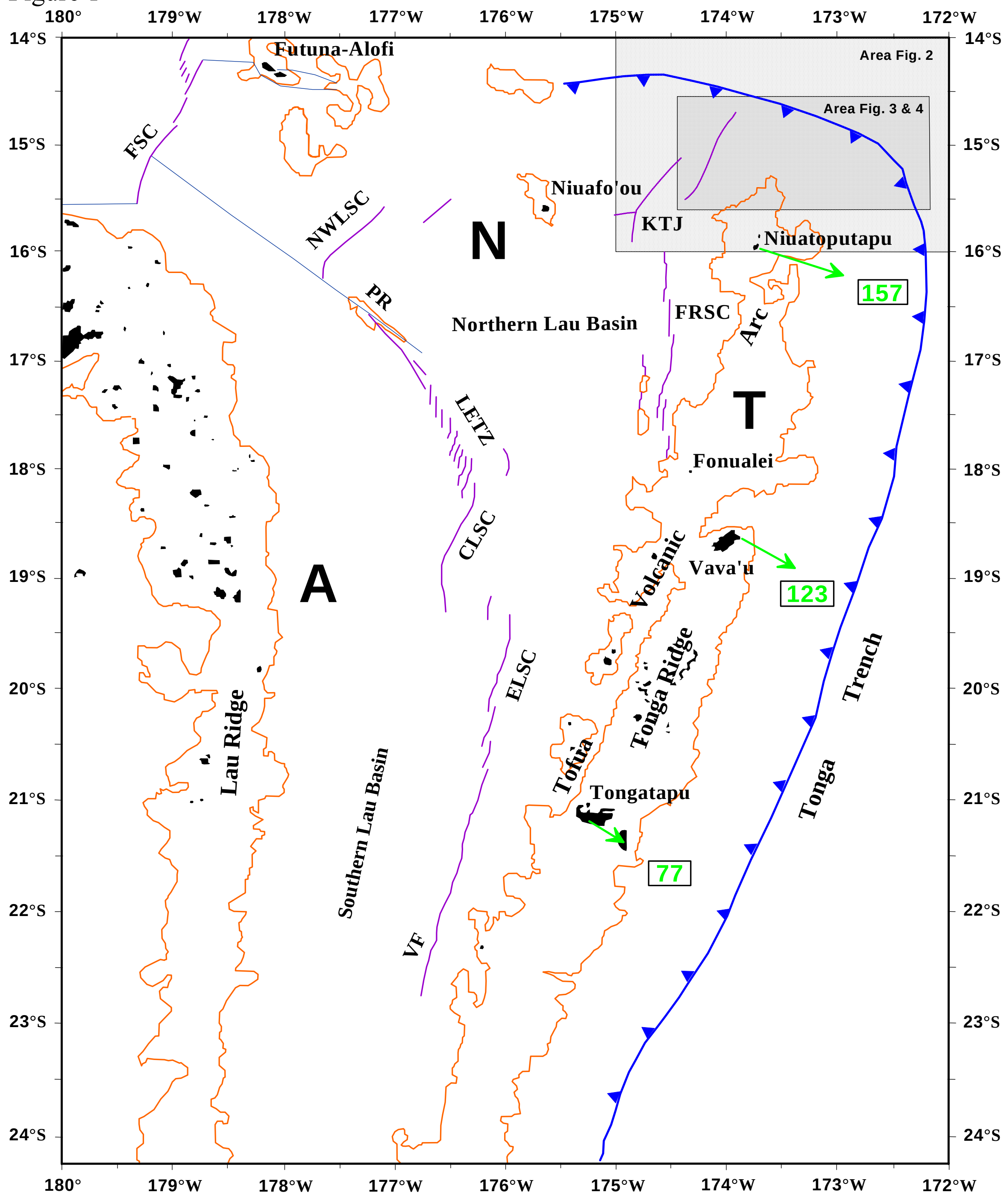

180°
179°W
178°W
177°W
176°W
175°W
174°W
173°W
172°W
14°S
15°S
16°S
17°S
18°S
19°S
20°S
21°S
22°S
23°S
24°S
Area Fig. 2
Area Fig. 3 & 4
Futuna-Alofi
FSC
NWLSC
PR
N
Niuafo'ou
KTJ
Niuatoputapu
157
Northern Lau Basin
FRSC
Arc
T
LETZ
Fonualei
CLSC
Volcanic
Vava'u
123
A
Tonga Ridge
ELSC
Lau Ridge
Tofua
Tongatapu
Southern Lau Basin
77
VF
Trench
Tonga

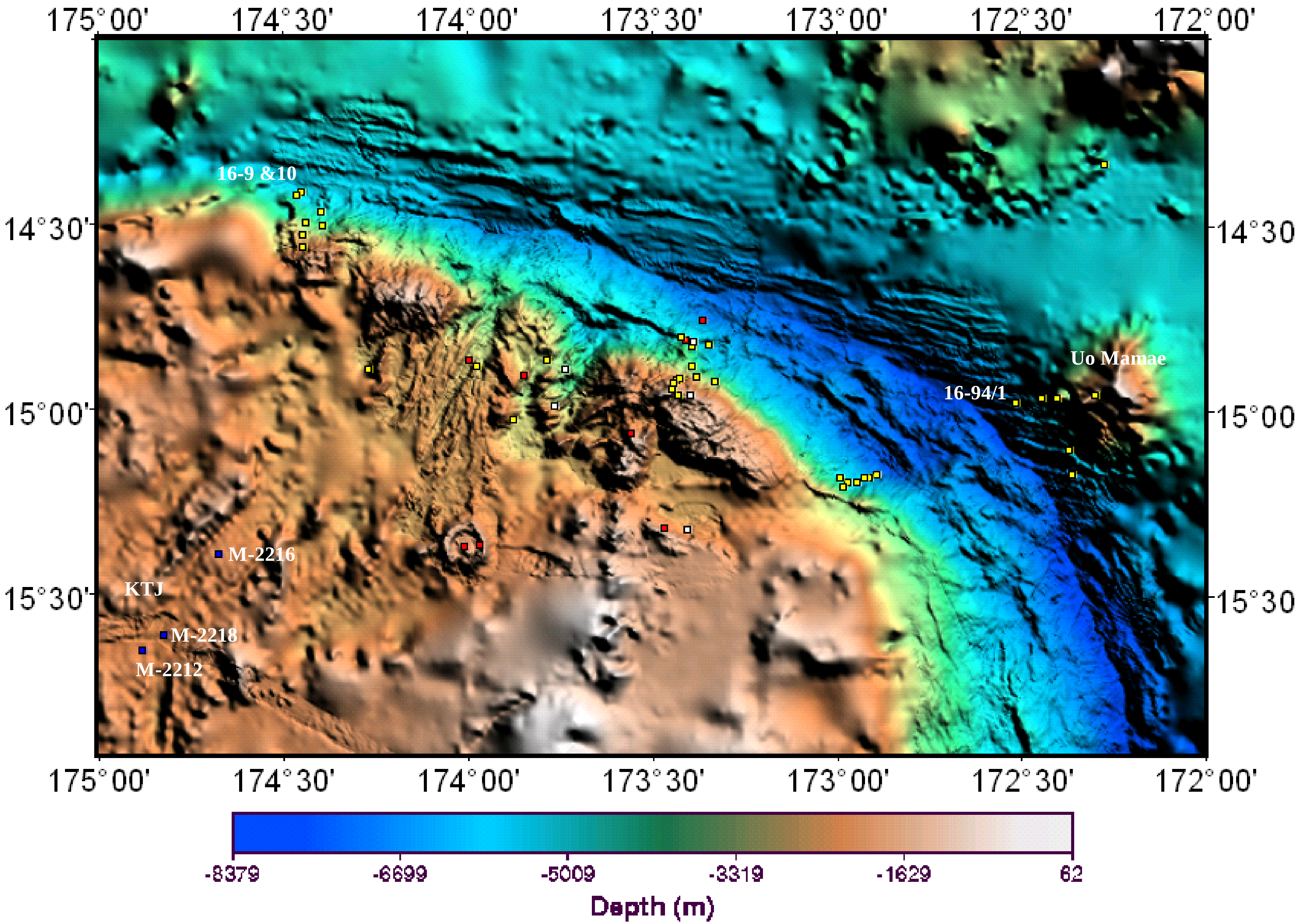
175°00'
174°30'
174°00'
173°30'
173°00'
172°30'
172°00'
14°30'
15°00'
15°30'
16-9 &10
Uo Mamae
16-94/1
M-2216
KTJ
M-2218
M-2212
-8379
-6699
-5009
-3319
-1629
62
Depth (m)

Figure 3

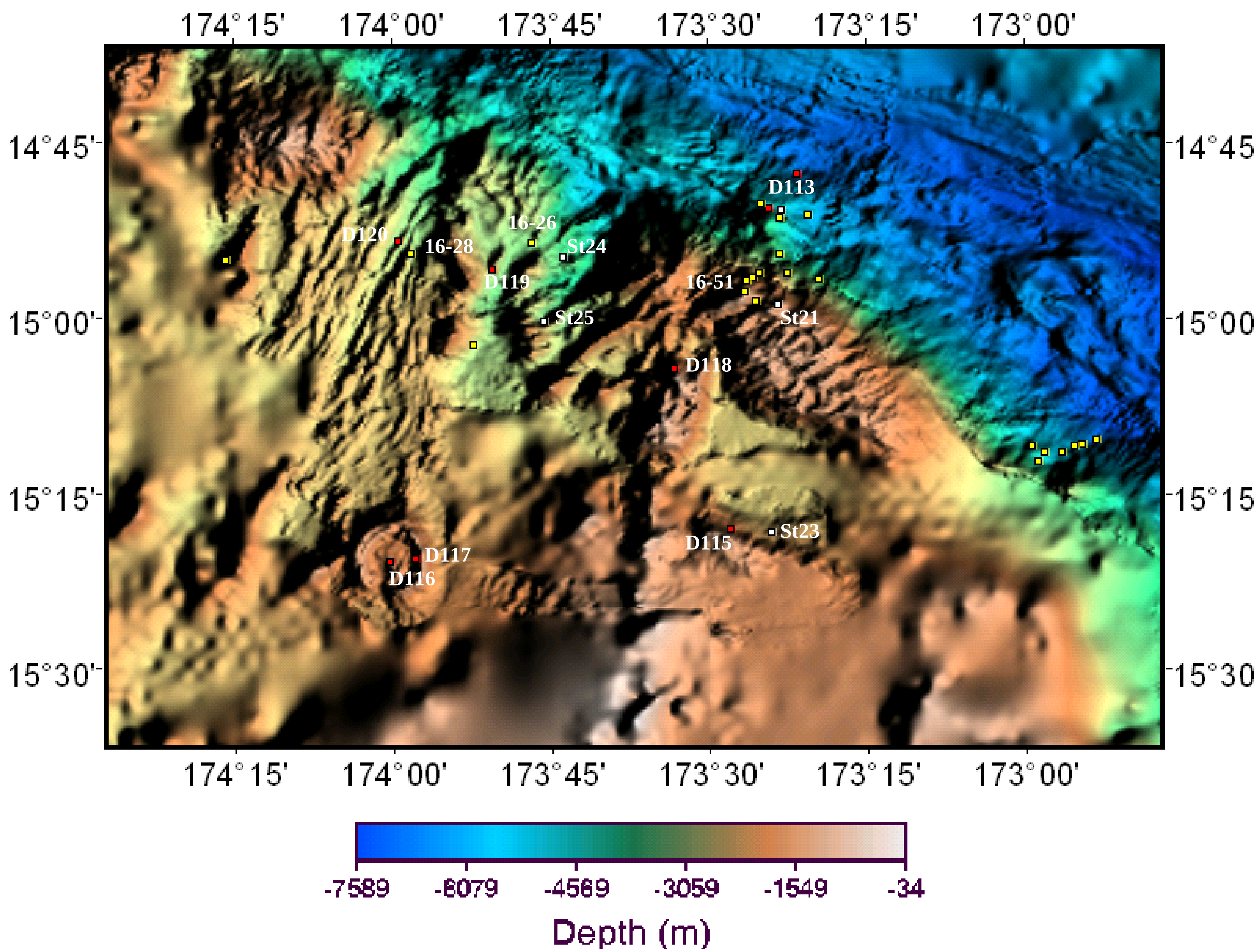
174° 15'
174° 00'
173° 45'
173° 30'
173° 15'
173° 00'
14°45'
15°00'
15°15'
15°30'
D113
D120
16-28
16-26
St24
D119
16-51
St25
St21
D118
D115
St23
D117
D116
-7589
-6079
-4569
-3059
-1549
-34
Depth (m)

Figure 4

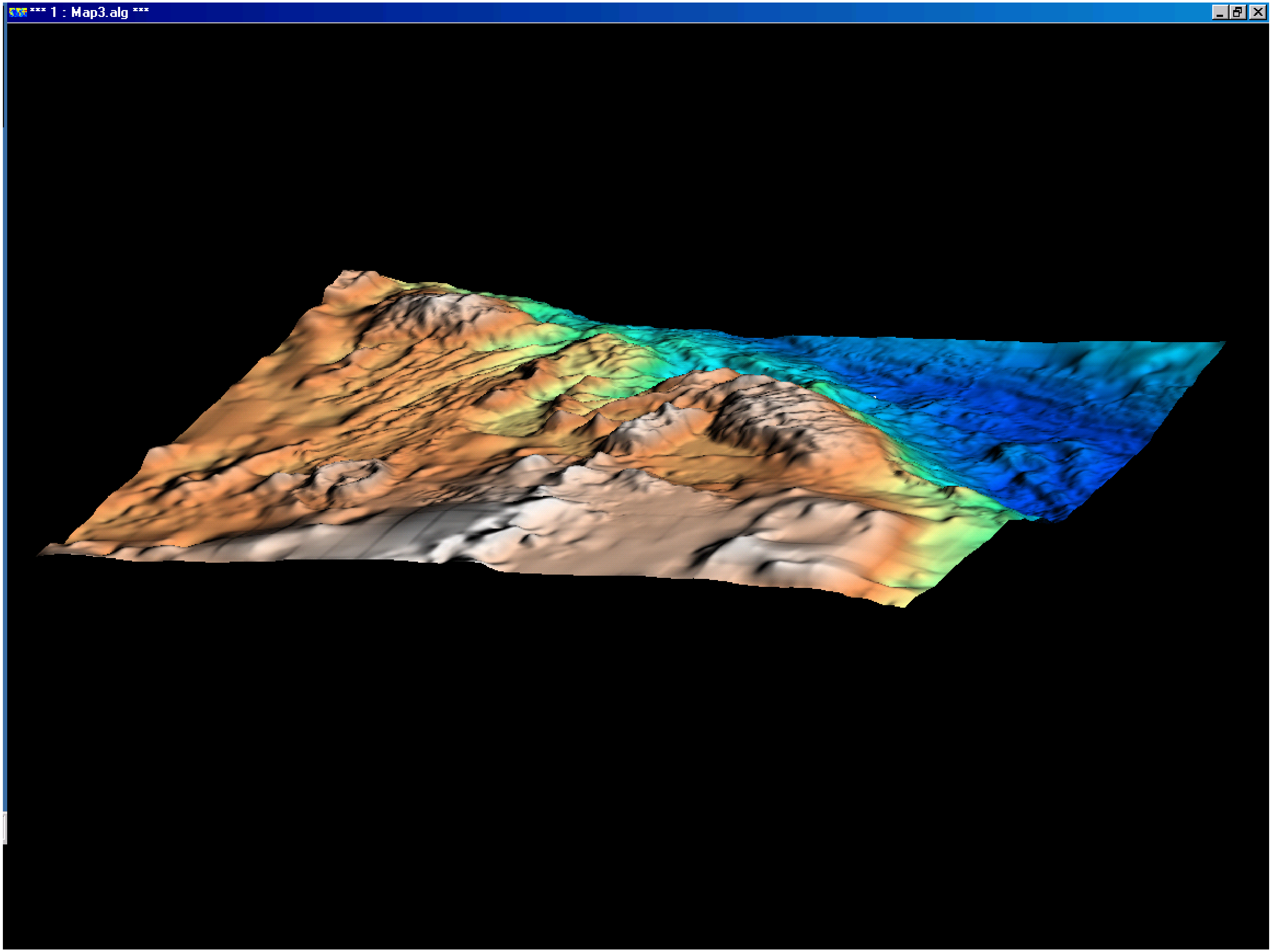

Figure 5

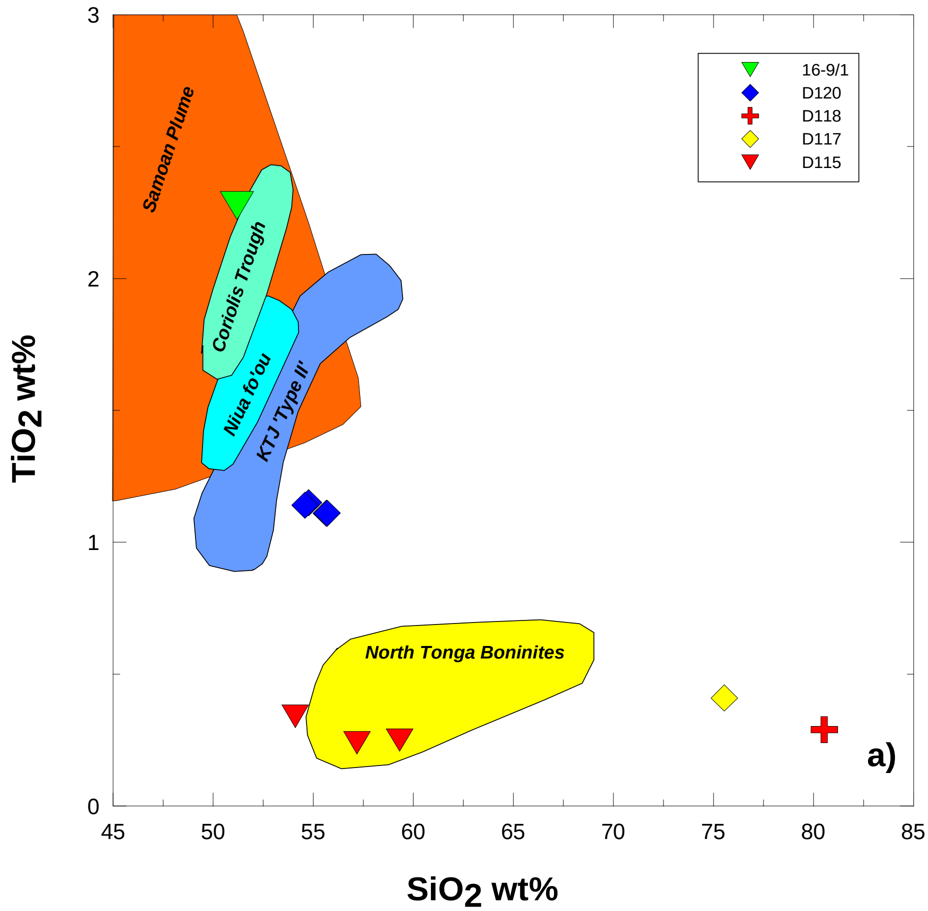

16-9/1
D120
D118
D117
D115
Samoan Plume
Coriolis Trough
Niua fo'ou
KTJ 'Type II'
North Tonga Boninites
a)
TiO2 wt%
SiO2 wt%
0
1
2
3
45
50
55
60
65
70
75
80
85

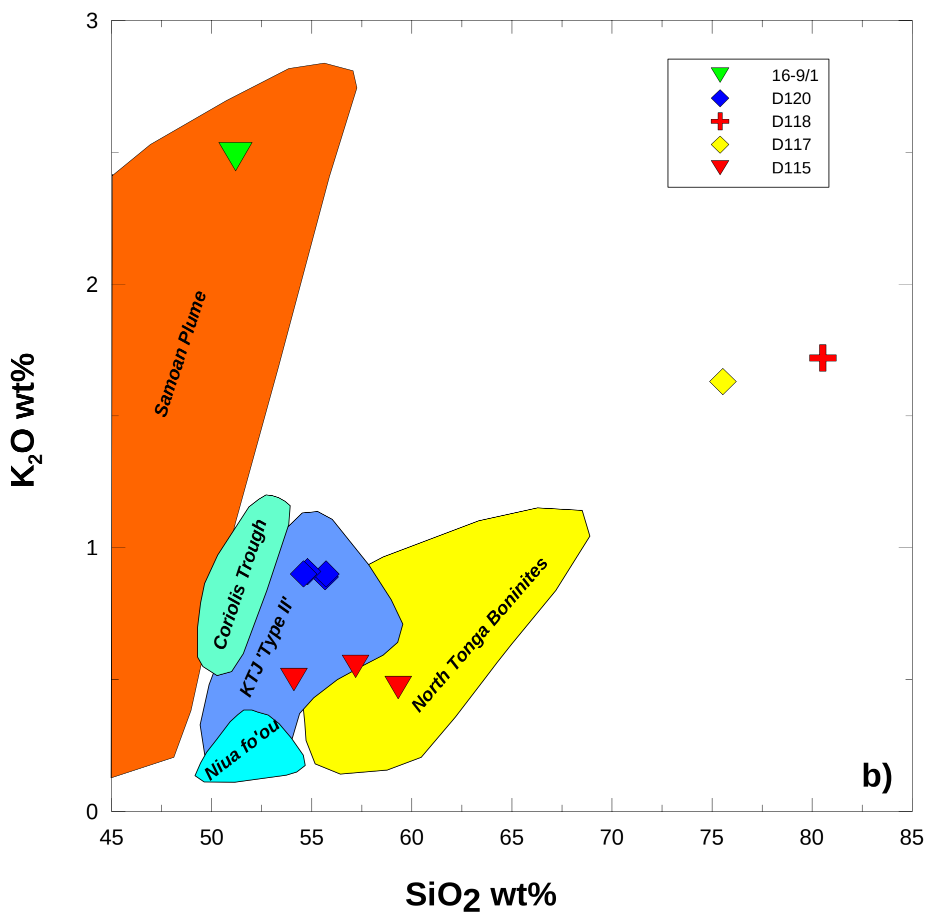

16-9/1
D120
D118
D117
D115
Samoan Plume
Coriolis Trough
KTJ 'Type II'
Niua fo'ou
North Tonga Boninites
b)
K2O wt%
SiO2 wt%
0
1
2
3
45
50
55
60
65
70
75
80
85

Figure 6

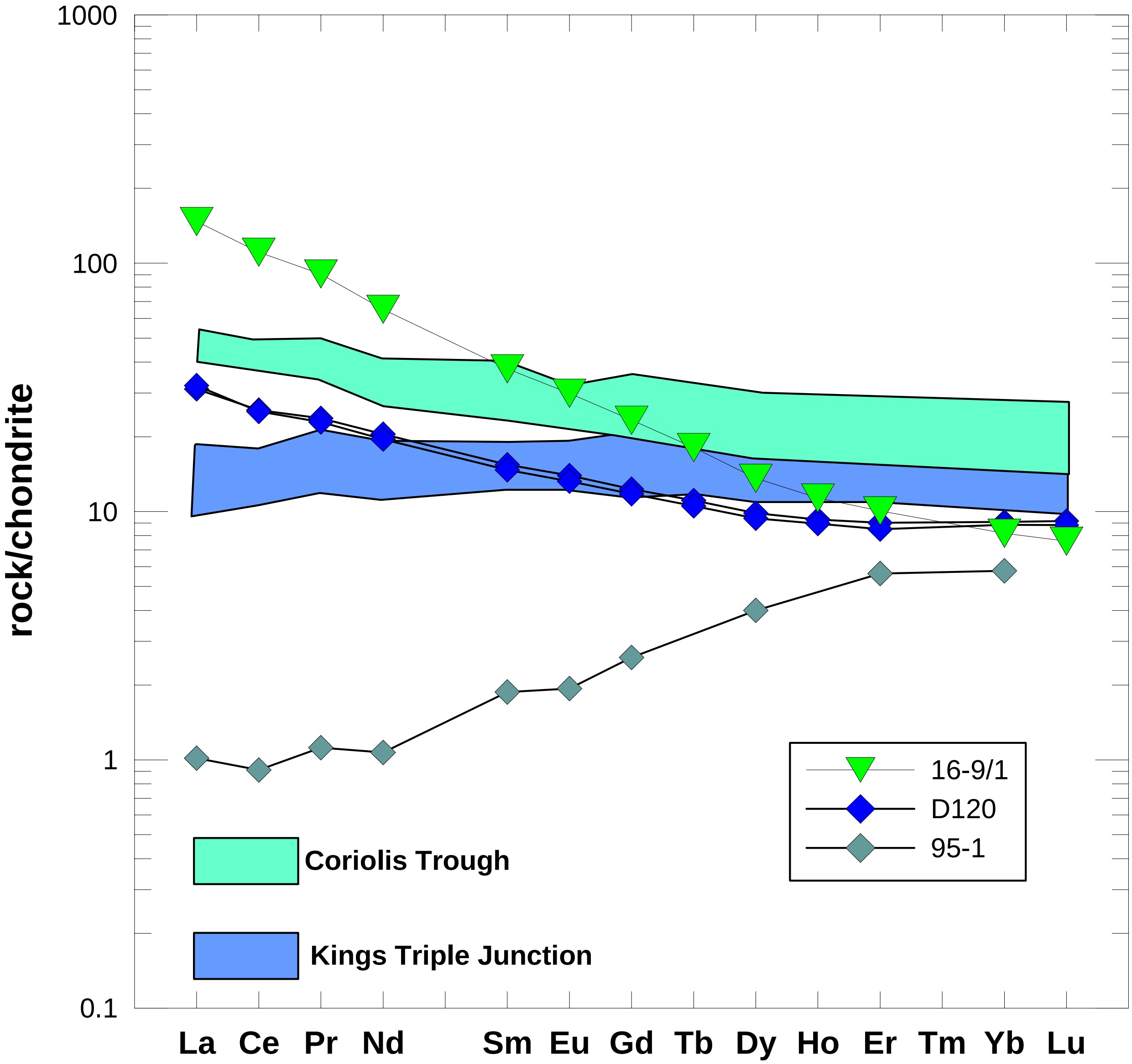
1000
100
10
1
0.1
rock/chondrite
La
Ce
Pr
Nd
Sm
Eu
Gd
Tb
Dy
Ho
Er
Tm
Yb
Lu
16-9/1
D120
95-1
Coriolis Trough
Kings Triple Junction

Figure 7

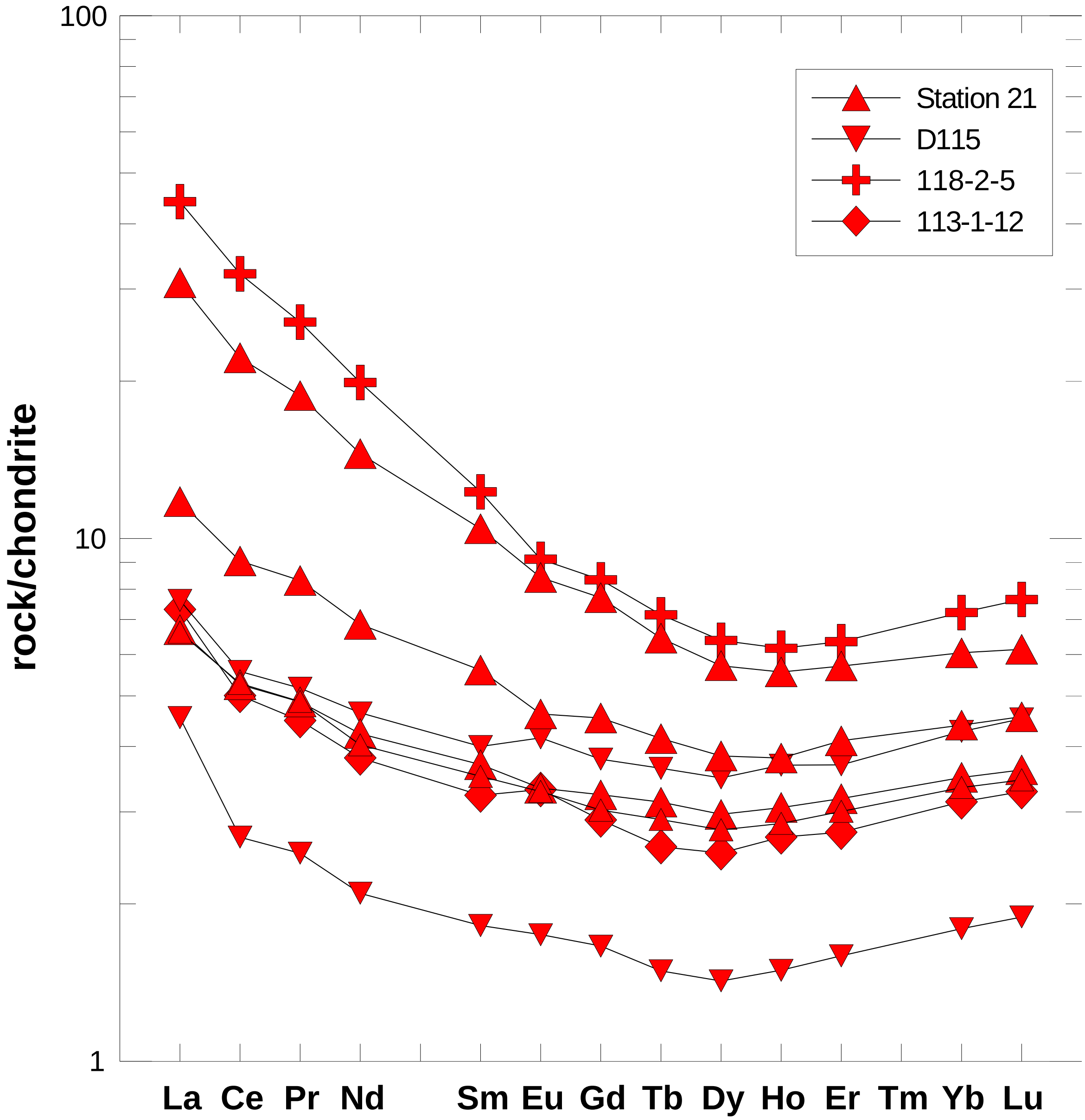

100
10
1
rock/chondrite
Station 21
D115
118-2-5
113-1-12
La
Ce
Pr
Nd
Sm
Eu
Gd
Tb
Dy
Ho
Er
Tm
Yb
Lu

Figure 8

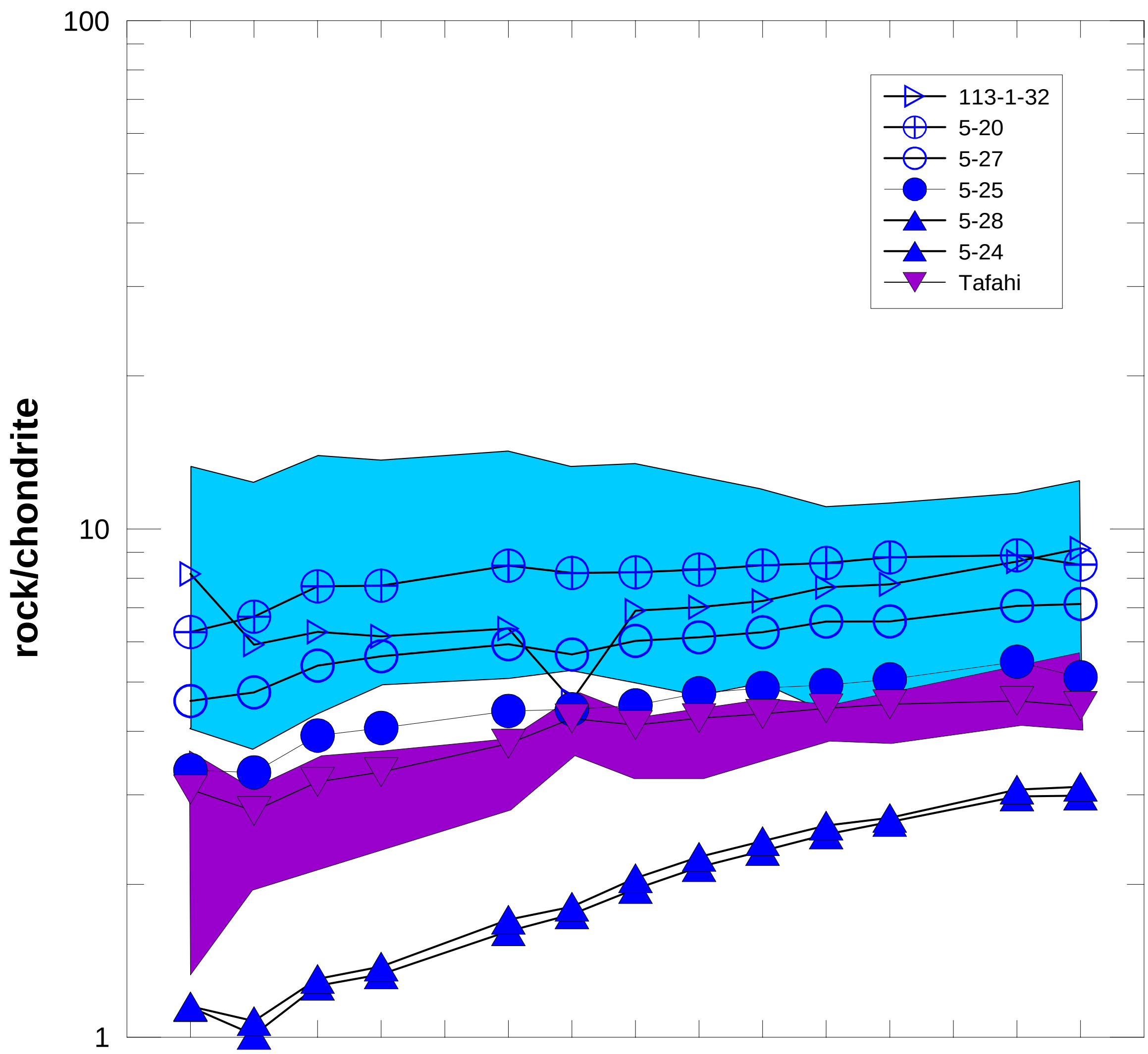

100
10
1
rock/chondrite
La
Ce
Pr
Nd
Sm
Eu
Gd
Tb
Dy
Ho
Er
Tm
Yb
Lu
113-1-32
5-20
5-27
5-25
5-28
5-24
Tafahi

Figure 9

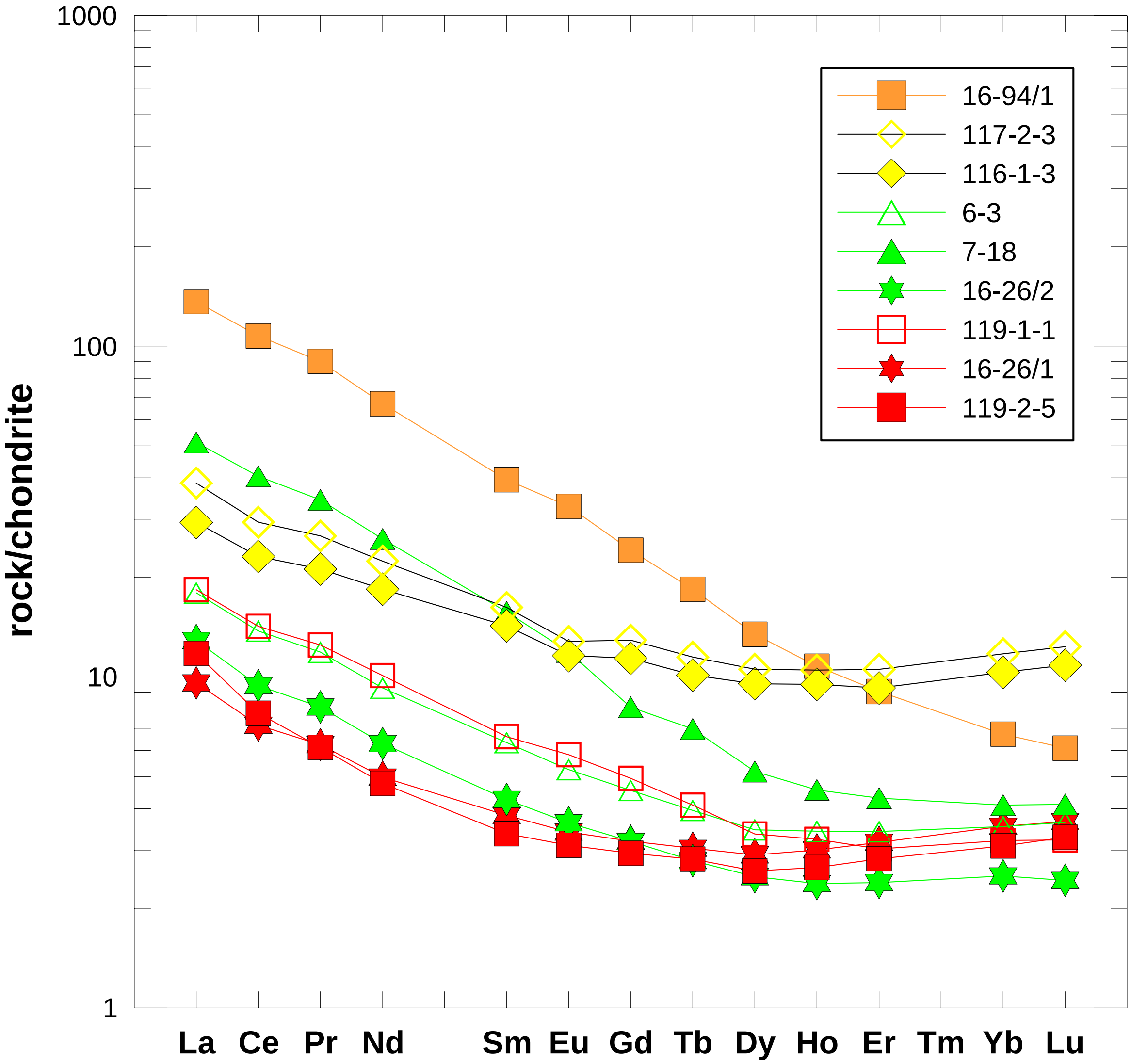
1000
100
10
1
rock/chondrite
La
Ce
Pr
Nd
Sm
Eu
Gd
Tb
Dy
Ho
Er
Tm
Yb
Lu
16-94/1
117-2-3
116-1-3
6-3
7-18
16-26/2
119-1-1
16-26/1
119-2-5

Figure 10

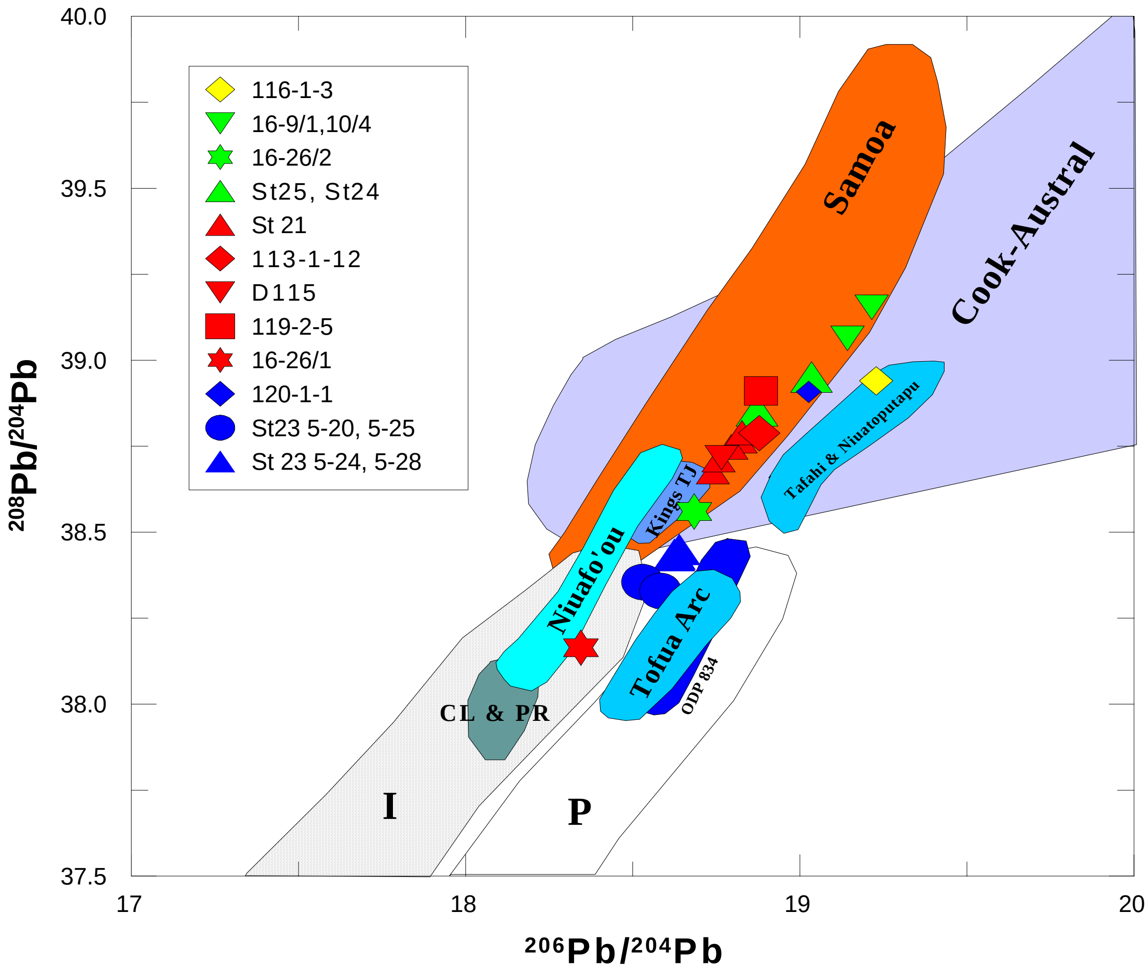

40.0
39.5
39.0
38.5
38.0
37.5
17
18
19
20
$^{208}Pb/^{204}Pb$
$^{206}Pb/^{204}Pb$
116-1-3
16-9/1,10/4
16-26/2
St25, St24
St 21
113-1-12
D115
119-2-5
16-26/1
120-1-1
St23 5-20, 5-25
St 23 5-24, 5-28
Samoa
Cook-Austral
Tafahi & Niuatoputapu
Kings TJ
Niuafo'ou
Tofua Arc
ODP 834
CL & PR
I
P

Figure 11

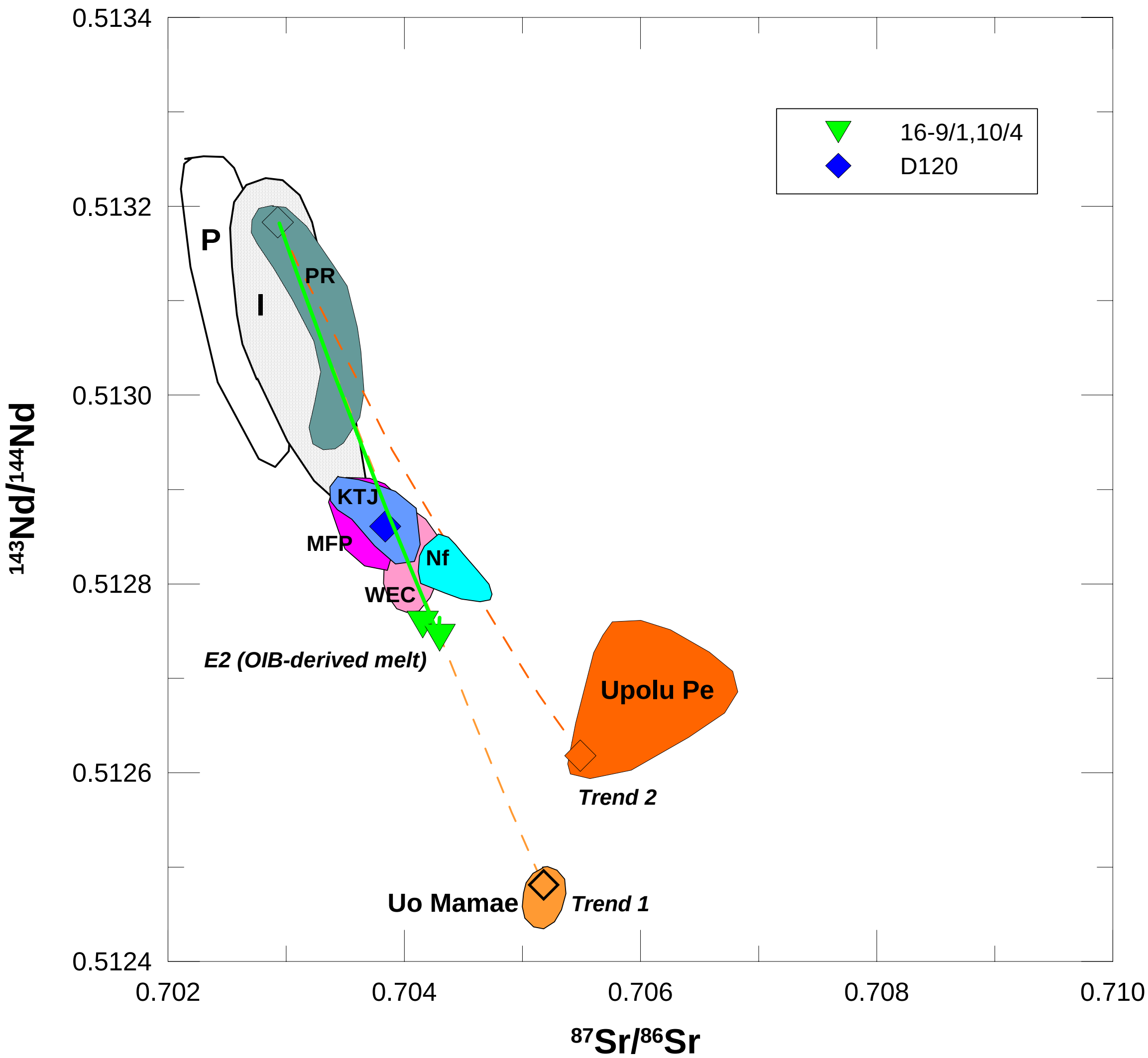

16-9/1,10/4
D120
P
I
PR
KTJ
MFP
Nf
WEC
E2 (OIB-derived melt)
Upolu Pe
Trend 2
Uo Mamae
Trend 1
0.5134
0.5132
0.5130
0.5128
0.5126
0.5124
0.702
0.704
0.706
0.708
0.710
$^{143}Nd/^{144}Nd$
$^{87}Sr/^{86}Sr$

Figure 12

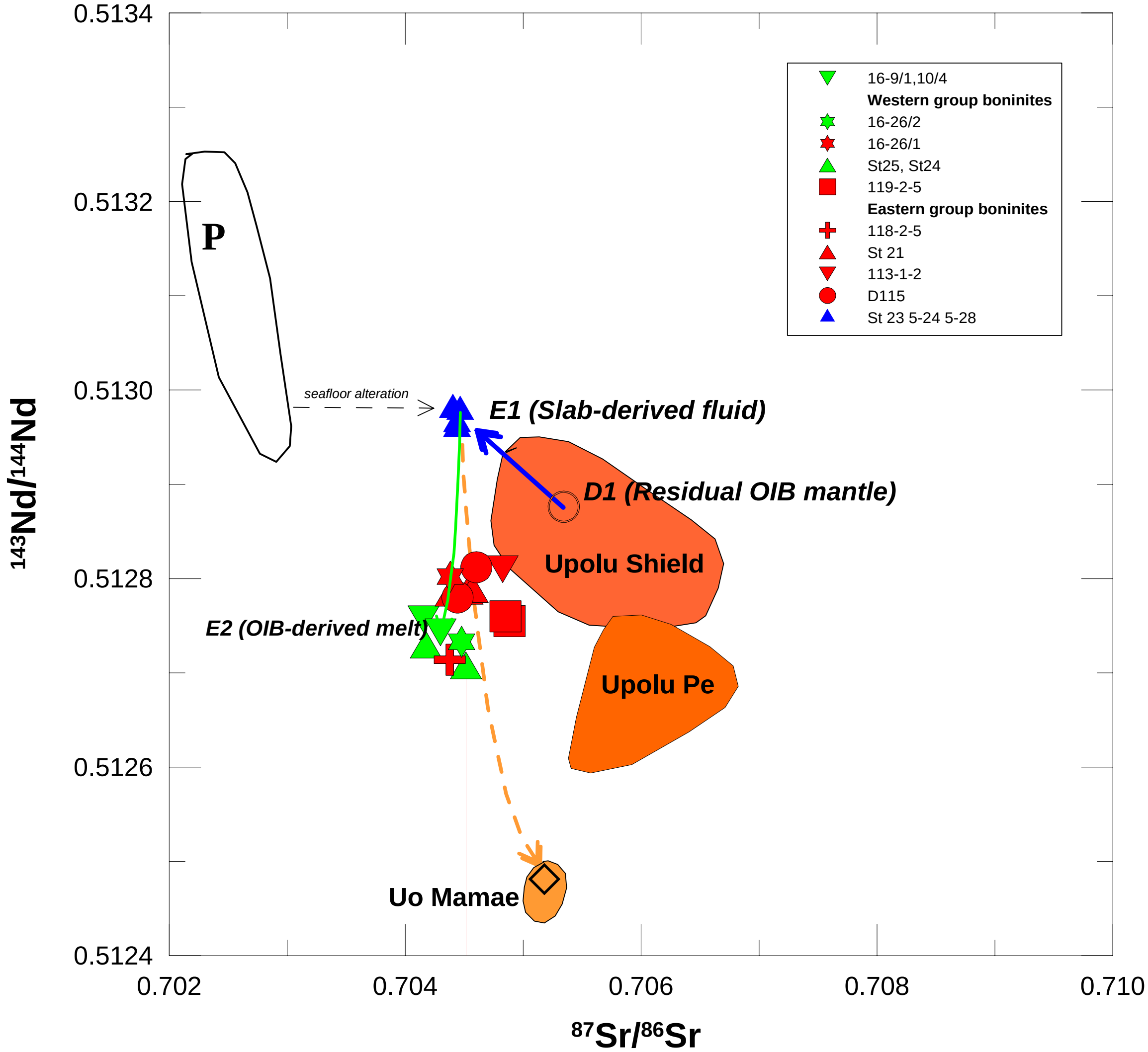

0.5134
0.5132
0.5130
0.5128
0.5126
0.5124
0.702
0.704
0.706
0.708
0.710
143Nd/144Nd
87Sr/86Sr
P
seafloor alteration
E1 (Slab-derived fluid)
D1 (Residual OIB mantle)
Upolu Shield
Upolu Pe
E2 (OIB-derived melt)
Uo Mamae
16-9/1,10/4
Western group boninites
16-26/2
16-26/1
St25, St24
119-2-5
Eastern group boninites
118-2-5
St 21
113-1-2
D115
St 23 5-24 5-28

Figure 13

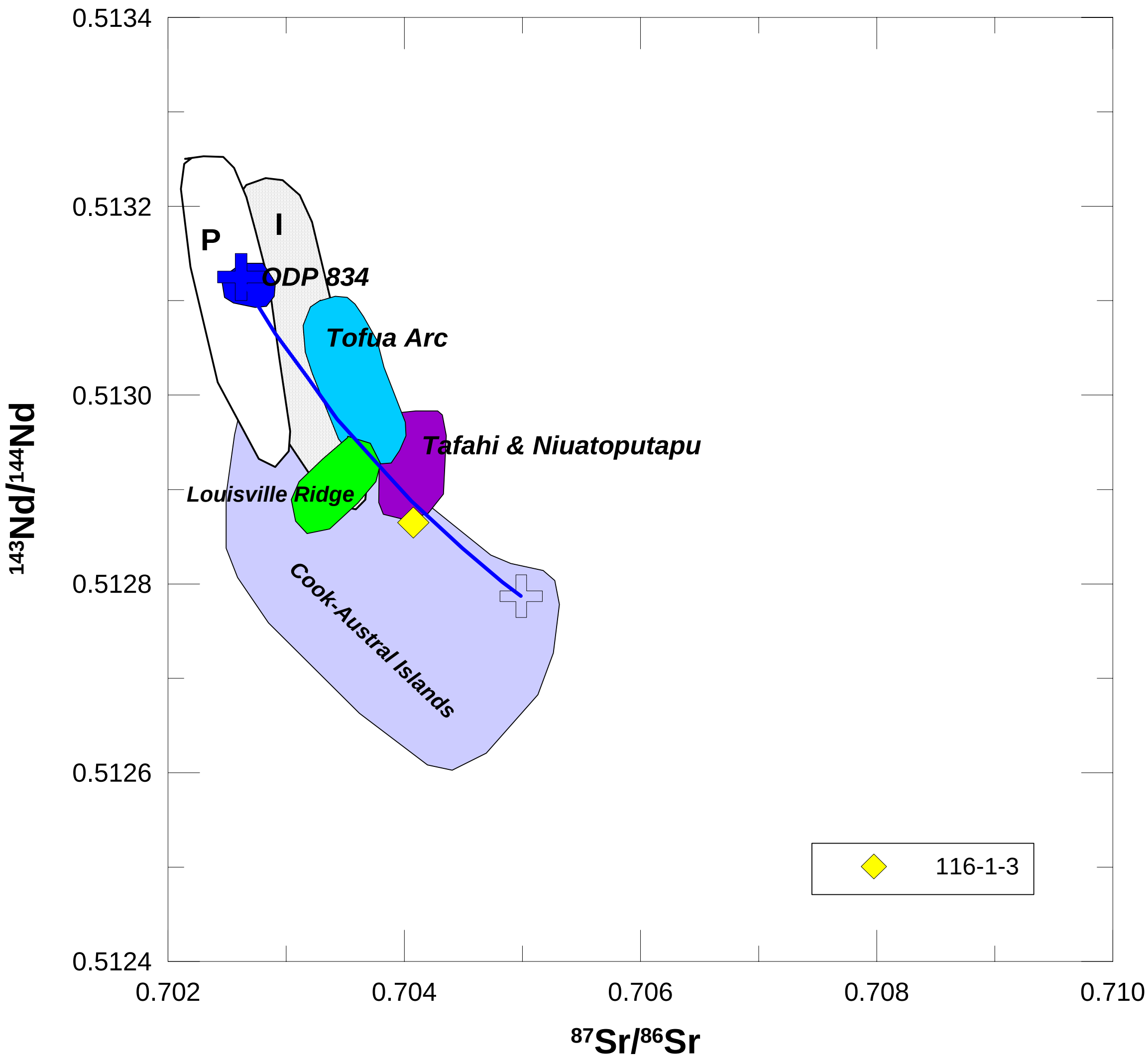

0.5134
0.5132
0.5130
0.5128
0.5126
0.5124
$^{143}Nd/^{144}Nd$
0.702
0.704
0.706
0.708
0.710
$^{87}Sr/^{86}Sr$
P
I
ODP 834
Tofua Arc
Tafahi & Niuatoputapu
Louisville Ridge
Cook-Austral Islands
116-1-3

Figure 14

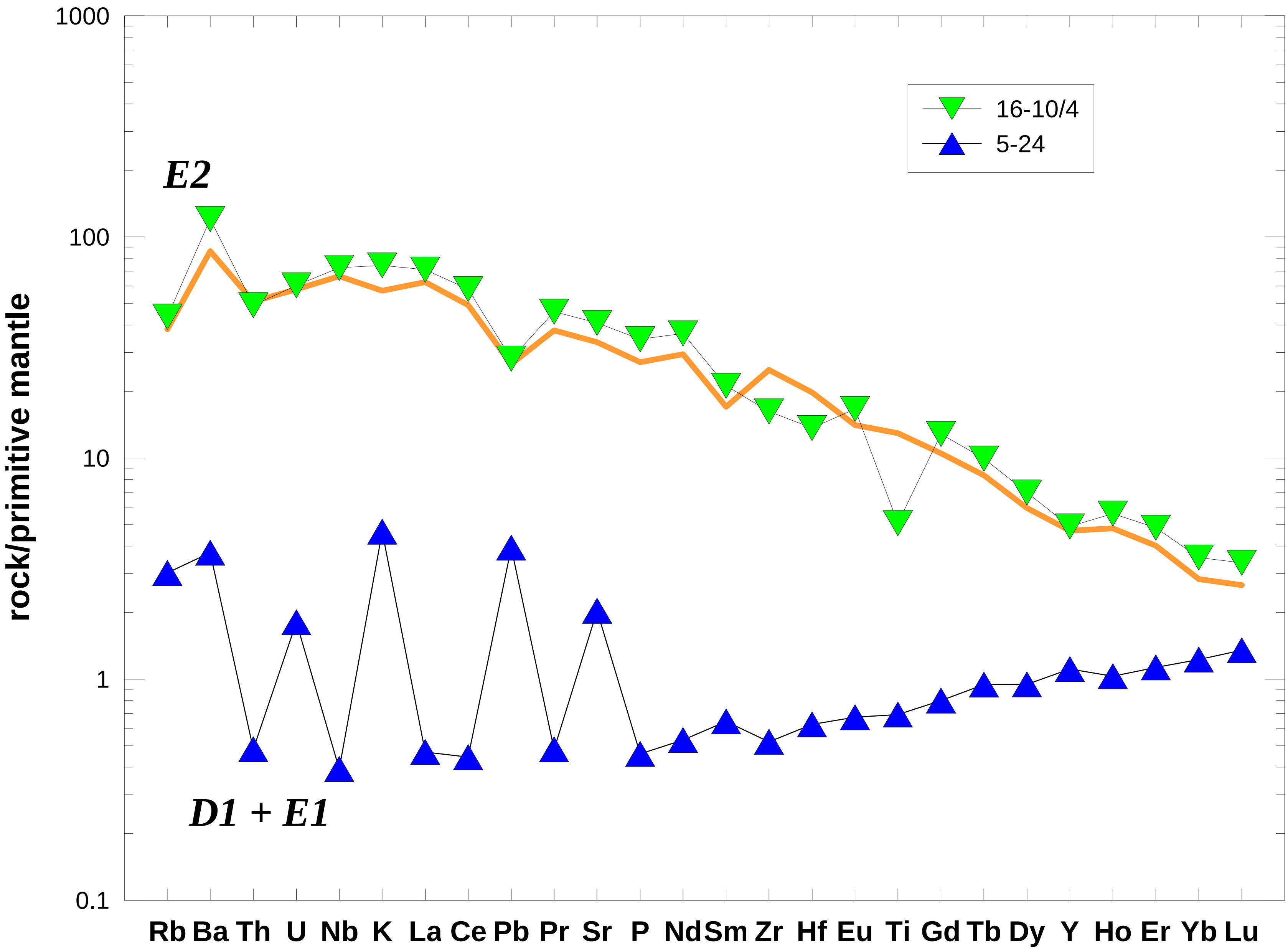

1000
100
10
1
0.1
rock/primitive mantle
E2
D1 + E1
16-10/4
5-24
Rb Ba Th U Nb K La Ce Pb Pr Sr P Nd Sm Zr Hf Eu Ti Gd Tb Dy Y Ho Er Yb Lu

Figure 15

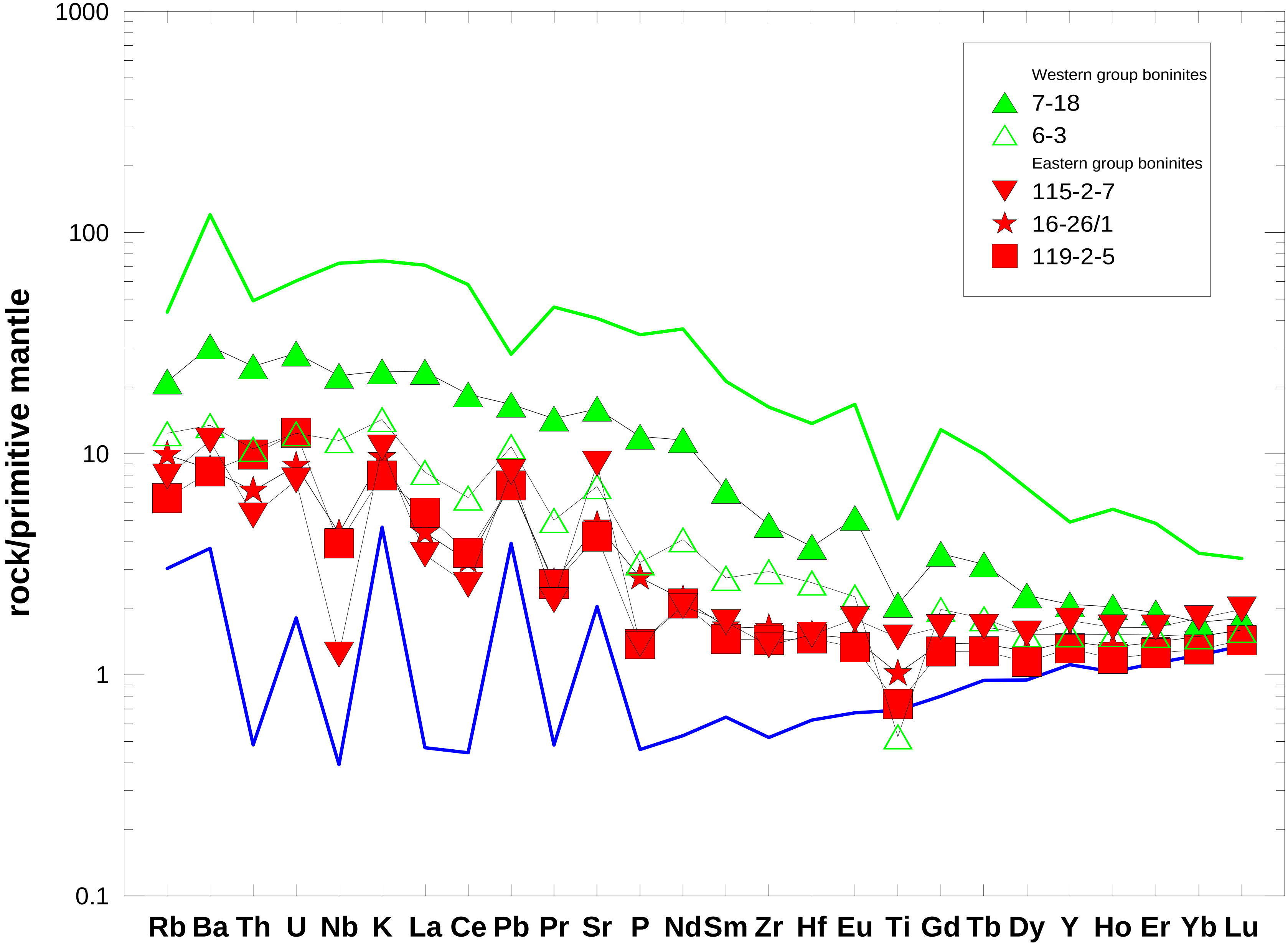

1000
100
10
1
0.1
rock/primitive mantle
Western group boninites
7-18
6-3
Eastern group boninites
115-2-7
16-26/1
119-2-5
Rb Ba Th U Nb K La Ce Pb Pr Sr P Nd Sm Zr Hf Eu Ti Gd Tb Dy Y Ho Er Yb Lu

Figure 16

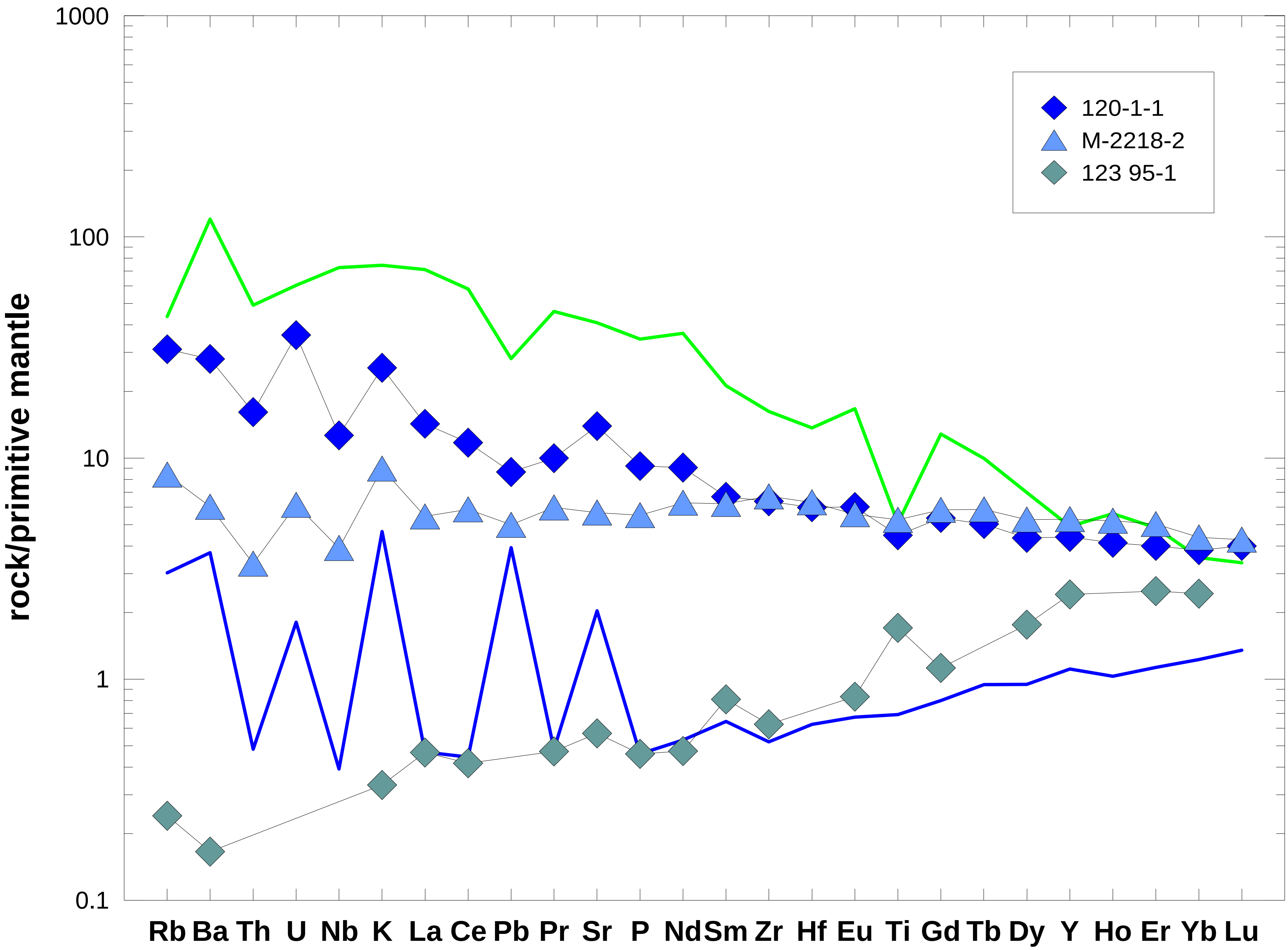

1000
100
10
1
0.1
rock/primitive mantle
120-1-1
M-2218-2
123 95-1
Rb Ba Th U Nb K La Ce Pb Pr Sr P Nd Sm Zr Hf Eu Ti Gd Tb Dy Y Ho Er Yb Lu

Table 1. Summary of dredging results in the northern Lau Basin – Tonga area during Boomerang Leg 8 of the R/V Melville in 1996

Station	Location/Comments	Start Latitude (°S)	Longitude (°W)	Depth (m)	Finish Latitude (°S)	Longitude (°W)	Depth (m)	Recovery/Deck Log
D113	Tonga Trench slope.	14 48.68	173 24.10	4496	14 49.21	173 24.42	1415	260kg of mostly diverse altered volcanics and diabases with minor gabbros, serpentinite and volcaniclastic sediments.
D115	North end of Tonga Ridge, north facing fault wall, just east of active arc.	15 18.7	173 27.49	2128	15 19.85	173 28.06	1200	260kg of vesicular oliv-phyric and plag-phyric volcanics.
D116	Central edifice of 10km wide caldera, about 40km west of Tofua Arc.	15 22.24	174 00.19	1541	15 22.58	174 00.19	1327	350-400kg of glassy andesitic to dacitic flow pieces.
D117	Eastern caldera wall of caldera.	15 22.10	173 58.18	1793	15 22.1	173 57.46	1339	800kg of dacitic-rhyolitic material.
D118	Northernmost seamount in Tofua Arc.	15 03.78	173 32.92	1380	15 04.24	173 33.18	900	500kg of plag-, quartz-phyric rhyolite, pumice.
D119	West side of NNE trending graben cutting trench slope. West side of a structure which parallels the north arm of the Lau spreading center.	14 54.99	173 50.31	3173	14 54.20	173 50.6	2613	400kg of oliv-phyric boninites. Picritic to basaltic in character.
D120	Northernmost arm of NE limb of King's Triple Junction ridges. Volcanic part of rift.	14 51.79	173 59.1	3084	14 52.11	173 59.75	2929	65kg of slightly Mn-coated and weathered glassy basalts, both pillow and more tabular, pahoehoe type pieces.

Table 2. Radiometric Age determinations for rock samples dredged from the northern Lau Basin – Tonga area.

Sample	Rock type	Lab/Data source	Method	Age (Ma)	(±) 1σ
Kallisto 82					
16-51/9	boninite	Acland [1996]	K-Ar	2.54	0.74
16-51/16	boninite	Acland [1996]	K-Ar	3.09	0.48
16-26/1	boninite	Acland [1996]	K-Ar	0.58	0.20
16-26/2	boninite	Acland [1996]	K-Ar	0.89	0.04
Natsushima 84					
3-23	boninite	OSU	K-Ar	1.40	0.03
5-27	basaltic andesite	OSU	K-Ar	2.03	0.11
Tafahi					
TT1	basaltic andesite	UCSC	K-Ar	0	0
Niuatoputapu					
TN3	basaltic andesite	UCSC	K-Ar	3.00	0.10

Table 3. Major (in wt%) and trace element (in ppm) geochemistry of samples recovered by dredging during R/V Melville 96 Boomerang Leg 8

Sample	113-1-12	113-1-30	113-1-24	113-1-32	115-1-1	115-1-2	115-1-8	115-1-5	115-2-5	115-2-7
Lithology	Boninite	Boninite	Boninite	Rhyolite	Boninite	Boninite	Boninite	Boninite	Andesite	Andesite
SiO_2	53.22	55.59	54.15	76.71	54.83	54.75	56.57	56.40	56.71	56.99
TiO_2	0.24	0.30	0.22	0.33	0.12	0.15	0.21	0.17	0.31	0.32
Al_2O_3	11.45	14.87	11.29	10.55	6.29	8.20	12.33	9.91	16.93	16.44
FeO*	9.10	8.25	9.86	4.98	9.03	10.07	10.33	10.60	9.77	9.88
MnO	0.16	0.13	0.18	0.08	0.20	0.21	0.19	0.21	0.17	0.17
MgO	13.37	9.19	14.02	1.08	17.29	14.62	8.29	10.28	3.66	3.82
CaO	8.85	8.92	9.42	1.72	11.55	11.04	10.52	11.17	10.74	10.61
Na_2O	2.66	1.83	0.77	4.35	0.52	0.71	1.15	0.90	1.32	1.42
K_2O	0.93	0.89	0.09	0.11	0.16	0.22	0.36	0.34	0.35	0.32
P_2O_5	0.02	0.03	0.02	0.07	0.01	0.01	0.03	0.02	0.03	0.03
LOI	6.22	8.36	7.42	2.08	0.00	0.24	0.69	0.51	0.02	0.00
Total†	99.58	99.42	99.74	99.55	99.78	99.54	99.85	99.88	100.21	99.39
Rb	5.7	20.3	1.3	2.4	2.1	5.0	5.7	5.4	5.2	5.0
Ba	119	112	24	38	44	58	79	87	79	80
Nb	1.0	1.2	1.2	1.7	<1.0	<1.0	1.3	1.4	1.3	<1.0
La	<2	<2	<2	4	<2	<2	2	3	2	2
Ce	<4	<4	<4	5	<4	<4	7	6	7	<4
Sr	123	78	88	87	81	106	201	157	201	190
Nd	4	<2	2	5	<2	3	3	5	3	2
Zr	13	14	9	37	7	8	15	11	15	15
Y	6	6	4.4	16	4	2.8	5	4.8	7	8
V	265	295	232	65	202	244	386	276	386	365
Sc	44	48	39	19	51	56	45	59	45	48
Cr	812	477	947	23	1354	896	44	656	44	20
Ni	228	124	282	7	135	125	51	58	13	12

Table 3. continued

Sample	116-1-1	116-1-3	116-2-1	117-1-1	117-2-3	118-2-5	118-2-8	119-1-1	119-2-5	119-3-5	119-3-6
Lithology	Dacite	Dacite	Dacite	Rhyolite	Rhyolite	Rhyolite	Rhyolite	Boninite	Boninite	Boninite	Boninite
SiO_2	66.22	66.37	67.33	73.39	73.51	73.81	73.77	47.18	52.95	55.76	57.98
TiO_2	0.55	0.55	0.56	0.41	0.41	0.28	0.30	0.31	0.16	0.22	0.26
Al_2O_3	13.73	13.59	13.68	12.49	12.40	12.93	12.99	7.06	9.02	10.79	13.61
FeO*	7.42	7.48	6.70	4.35	4.33	3.29	3.28	8.59	8.37	8.67	7.52
MnO	0.14	0.14	0.12	0.09	0.10	0.07	0.07	0.15	0.16	0.16	0.14
MgO	1.76	1.73	1.72	0.65	0.65	1.09	1.12	28.70	20.79	13.87	8.33
CaO	5.66	5.62	5.50	3.16	3.21	3.61	3.59	6.60	7.29	8.88	9.89
Na_2O	3.33	3.33	3.23	3.47	3.61	3.41	3.38	0.98	0.98	1.33	1.77
K_2O	1.00	0.99	0.97	1.91	1.69	1.44	1.43	0.32	0.24	0.22	0.44
P_2O_5	0.19	0.19	0.17	0.08	0.09	0.06	0.06	0.09	0.03	0.08	0.06
LOI	0.96	1.08	1.17	3.08	1.67	1.47	1.36	0.08	0.91	0.05	0.37
Total†	99.97	99.62	99.50	99.66	99.78	100.28	99.94	99.80	99.81	99.70	99.86
Rb	17.1	17.7	16.8	30.6	30.1	28.4	28.8	7.0	4.0	30.0	7.4
Ba	227	227	233	355	361	342	337	102	58	71	99
Nb	5.9	6.1	5.6	8.2	7.9	15.8	15.7	5.3	3.0	4.4	5.9
La	8	11	9	12	15	16	13	7	6	9	8
Ce	21	23	18	26	27	28	29	15	8	13	15
Sr	244	244	252	227	224	242	238	138	89	141	158
Nd	13	13	10	15	17	15	14	7	5	7	6
Zr	57	57	58	74	75	75	76	21	15	19	30
Y	20	20	17	23	23	14	14	6	6	9	9
V	179	175	170	11	12	47	48	135	160	208	213
Sc	26	27	26	16	15	12	13	24	30	34	36
Cr	3	2	2	2	4	17	19	1957	1659	848	411
Ni	3	2	2	1	1	3	3	957	472	212	77

Table 3. continued

Sample	120-1-1	120-1-3	120-2-1	120-2-3
Lithology	Basalt	Basalt	Basalt	Basalt
SiO_2	53.18	53.30	53.98	54.07
TiO_2	0.97	0.98	0.90	0.90
Al_2O_3	16.91	16.83	16.90	16.90
FeO*	8.23	8.28	8.51	8.45
MnO	0.15	0.15	0.15	0.15
MgO	6.16	6.07	5.84	5.81
CaO	10.95	10.87	10.29	10.39
Na_2O	2.48	2.51	2.50	2.39
K_2O	0.77	0.80	0.74	0.76
P_2O_5	0.20	0.20	0.18	0.18
LOI	1.22	1.39	1.08	1.47
Total†	99.42	100.20	100.16	100.10
Rb	19.7	20.5	17.9	19.3
Ba	194	194	183	179
Nb	9.7	9.5	9.6	9.2
La	12	12	11	10
Ce	22	26	23	21
Sr	294	290	278	279
Nd	14	14	13	13
Zr	71	72	66	67
Y	20	21	20	19
V	262	259	292	296
Sc	33	33	34	34
Cr	84	85	34	33
Ni	51	51	44	44

Table 4. Major (in wt%) element geochemistry of glasses recovered by dredging during R/V Melville 96 Boomerang Leg 8

Sample	120-2-3	120-2-1	120-1-3	120-1-1	118-2-8	117-2-3	115-1-11	115-1-10	115-1-8
SiO_2	55.66	55.68	54.77	54.57	80.53	75.5	54.10	57.17	59.31
TiO_2	1.11	1.11	1.15	1.14	0.29	0.41	0.34	0.24	0.25
Al_2O_3	15.70	15.75	16.05	16.03	11.51	11.88	14.35	14.12	14.04
FeO	9.51	9.55	9.42	9.24	2.41	4.22	12.96	11.74	11.13
MnO	0.17	0.16	0.16	0.17	0.04	0.09	0.21	0.21	0.09
MgO	4.77	4.72	5.08	5.12	0.26	0.45	4.42	4.00	3.78
CaO	9.46	9.39	9.79	9.99	1.78	2.83	11.43	10.30	9.49
Na_2O	2.52	2.49	2.41	2.57	1.43	2.88	1.48	1.48	1.27
K_2O	0.89	0.90	0.91	0.90	1.72	1.63	0.50	0.55	0.47
P_2O_5	0.21	0.20	0.24	0.22	0.03	0.05	0.18	0.16	0.10
Cr_2O_3	0.00	0.01	0.02	0.02	0.00	0.02	0.03	0.01	0.06
NiO	0.01	0.03	0.02	0.02	0.00	0.02	0.03	0.01	0.0

Table 5. Trace (ppm) element geochemistry of rock samples dredged from the northern Lau Basin-Tonga area

Sample No	Lab	Li	Be	Sc	Ti	V	Cr	Co	Ni	Cu	Zn	Ga	As
Kallisto 82													
16-9/1	ANU	4.45	1.91	25.0	8731	198	559	46.2	230	51	91	17.1	1.02
16-10/4	ANU	5.34	1.75	28.8	12009	296	142	41.9	40	49	96	18.2	0.92
16-94/1	ANU	8.66	1.97	20.7	14132	202	612	50.6	285	51	107	18.4	1.24
16-26/1	ANU	5.23	0.26	32.7	1417	212	608	48.9	278	68	56	8.5	1.14
16-26/2	ANU	2.49	0.28	24.1	1384	126	809	78.8	695	41	51	5.6	0.36
Natsushima 84													
7-18	ANU	4.89	0.71	36.1	2617	220	592	46.3	210	75	61	10.1	1.24
6-3	ANU	5.08	0.40	25.1	2009	220	754	49.0	227	101	55	8.8	1.16
5-25	ANU	4.65	0.18	38.7	2001	212	613	101.7	324	70	63	8.6	0.71
	UTAS			43.1									
5-24	ANU	4.04	0.09	35.1	825	168	1180	71.9	569	57	60	6.1	1.25
	UTAS (2)			38.5									
5-28	UTAS (2)			40.2									
5-27	UTAS			41.4									
5-20	ANU	4.73	0.34	38.9	4022	280	134	34.2	70	82	67	13.7	1.63
	UTAS			35.9									
3-44	ANU	5.68	0.30	37.5	1272	228	1006	54.1	267	77	62	9.1	1.49
3-51	ANU	4.33	0.35	35.6	1712	345	532	43.9	113	85	57	11.2	0.72
3-24	ANU	6.53	0.43	18.7	1840	266	574	42.5	142	102	63	9.9	2.34
3-36	ANU	9.85	0.88	29.5	2760	289	102	25.3	20	132	65	14.9	2.02
11-3	UTAS												

Table 5. continued

Sample No	Lab	Li	Be	Sc	Ti	V	Cr	Co	Ni	Cu	Zn	Ga	As
Keldysh/Mir 90													
M-2212-2	ANU	4.31	0.50	40.2	7045	253	218	38.9	68	75	63	14.4	0.64
	BRIS												
M-2212-2g	ANU	5.18	0.52	36.3	6999	254	224	39.5	73	73	57	13.7	0.42
M-2218-1	BRIS												
M-2218-2	ANU	6.25	0.59	31.4	7974	267	149	41.2	112	56	67	14.0	0.37
	BRIS												
M-2218-3	BRIS												
M-2218-4	BRIS												
M-2218-4g	ANU	6.03	0.52	36.0	7831	237	318	43.5	115	66	66	15.1	0.36
M-2218-7	BRIS												
M-2218-8	BRIS												
M-2218-9	ANU	5.56	0.52	31.9	7761	232	309	41.7	114	65	64	14.4	0.33
	BRIS												
M-2218-10	ANU	5.00	0.49	38.5	6999	242	302	40.1	93	70	62	14.2	0.37
	BRIS												
M-2218-11	BRIS												
M-2218-12	BRIS												
Melville 96													
113-1-12	UTAS												
113-1-32	UTAS												
115-1-1	UTAS												
115-2-7	UTAS												
116-1-3	UTAS												
117-2-3	UTAS												
118-2-5	UTAS												
119-1-1	UTAS												
119-2-5	UTAS												
120-1-1	UTAS												
120-2-1	UTAS												

Table 5. continued

Sample No	Rb	Sr	Y	Zr	Nb	Cs	Ba
Kallisto 82							
16-9/1	37.52	689.1	23.24	180.15	45.504	0.906	688.1
16-10/4	27.66	862.1	22.32	181.99	51.717	0.631	842.1
16-94/1	24.28	705.2	21.35	280.36	47.396	0.180	603.1
16-26/1	6.27	100.5	6.44	18.19	3.113	0.173	59.4
16-26/2	6.80	96.8	5.30	20.54	4.005	0.137	63.9
Natsushima 84							
7-18	13.46	337.1	9.48	53.39	16.052	0.321	213.8
6-3	7.85	150.0	6.92	32.85	8.190	0.190	93.9
5-25	2.22	66.0	10.15	19.98	0.671	0.122	33.4
	2.35	70.6	9.32	20.46	0.650	0.119	32.8
5-24	1.92	43.0	5.06	5.83		0.111	26.1
	2.24	47.6	4.99	6.39	0.280	0.124	27.9
5-28	2.34	49.8	5.19	6.76	0.295	0.129	28.4
5-27	3.49	107.1	12.70	26.60	0.980	0.185	47.9
5-20	3.23	120.7	17.65	38.87	1.495	0.156	49.8
	2.91	126.2	16.20	38.72	1.170	0.146	49.7
3-44	6.15	143.5	6.36	12.61	2.060	0.245	92.1
3-51	5.42	166.7	5.63	13.21	1.630	0.062	98.4
3-24	9.46	167.2	8.15	19.66	1.873	0.313	128.0
3-36	18.08	377.1	12.15	43.83	4.592	0.535	265.1
11-3							

Table 5. continued

Sample No	Rb	Sr	Y	Zr	Nb	Cs	Ba
Keldysh/Mir 90							
M-2212-2	6.01	135.3	25.31	59.93	2.383	0.135	40.6
M-2212-2g	6.06	127.0	22.30	60.38	2.430	0.109	39.6
M-2218-1							
M-2218-2	5.35	119.6	24.06	75.19	2.791	0.135	42.1
M-2218-3							
M-2218-4							
M-2218-4g	2.47	130.1	27.01	72.08	2.243	0.036	23.7
M-2218-7							
M-2218-8							
M-2218-9	2.37	122.9	23.67	70.93	2.256	0.041	24.6
M-2218-10	4.86	120.3	24.86	60.91	2.140	0.109	31.1
M-2218-11							
M-2218-12							
Melville 96							
113-1-12				13.5	1.06	0.007	125.3
113-1-32				39.9	1.62	0.041	40.7
115-1-1				7.5	0.41	0.084	37.5
115-2-7				15.2	0.88	0.148	76
116-1-3				59.7	5.46	0.365	233.8
117-2-3				77.2	7.61	0.634	357.5
118-2-5				76.3	14.97	0.691	335.1
119-1-1				22.6	4.56	0.133	95.8
119-2-5				16.1	2.8	0.146	53.4
120-1-1				71.3	9.03	0.343	196.1
120-2-1				66.9	9.34	0.307	186.5

Table 5. continued

Sample No	La	Ce	Pr	Nd	Sm	Eu	Gd	Tb	Dy	Ho	Er	Tm	Yb	Lu
Kallisto 82														
16-9/1	46.352	90.105	10.497	38.987	7.214	2.163	6.040	0.888	4.424	0.827	2.143		1.702	0.245
16-10/4	48.884	103.091	12.669	49.566	9.421	2.799	7.657	1.073	5.144	0.920	2.323		1.749	0.249
16-94/1	42.938	87.271	10.436	39.988	7.580	2.369	6.263	0.903	4.378	0.788	1.928		1.398	0.197
16-26/1	3.024	5.813	0.724	2.973	0.734	0.245	0.827	0.149	0.942	0.219	0.675		0.736	0.118
16-26/2	4.065	7.660	0.942	3.756	0.819	0.262	0.825	0.137	0.810	0.174	0.510		0.521	0.079
Natsushima 84														
7-18	16.117	32.904	3.978	15.613	3.022	0.860	2.101	0.341	1.685	0.333	0.917		0.853	0.133
6-3	5.662	11.215	1.381	5.530	1.218	0.379	1.178	0.194	1.123	0.250	0.727		0.735	0.118
5-25	1.021	2.720	0.442	2.325	0.827	0.312	1.189	0.234	1.521	0.355	1.080		1.095	0.175
	1.057	2.699	0.455	2.424	0.842	0.319	1.165	0.233	1.582	0.360	1.078	0.160	1.140	0.165
5-24	0.322	0.788	0.133	0.718	0.286	0.113	0.477	0.102	0.698	0.169	0.543		0.605	0.100
	0.361	0.822	0.147	0.794	0.311	0.126	0.508	0.106	0.756	0.183	0.565	0.085	0.620	0.097
5-28	0.363	0.876	0.151	0.823	0.327	0.131	0.533	0.111	0.791	0.191	0.576	0.088	0.639	0.101
5-27	1.445	3.878	0.625	3.354	1.139	0.409	1.561	0.300	2.037	0.480	1.402	0.207	1.469	0.230
5-20	2.031	5.441	0.880	4.571	1.569	0.573	2.157	0.416	2.680	0.614	1.862		1.851	0.287
	1.976	5.467	0.895	4.620	1.627	0.592	2.130	0.408	2.757	0.626	1.874	0.263	1.846	0.275
3-44	2.108	4.271	0.565	2.527	0.709	0.240	0.837	0.153	0.965	0.223	0.677		0.726	0.117
3-51	2.085	4.294	0.566	2.406	0.673	0.237	0.783	0.142	0.901	0.208	0.640		0.695	0.112
3-24	3.707	7.365	0.964	4.088	1.076	0.333	1.175	0.203	1.247	0.278	0.874		0.914	0.147
3-36	9.722	18.027	2.176	8.673	2.005	0.608	1.995	0.316	1.856	0.406	1.214		1.257	0.198
11-3[a]	*1.08*		*0.64*	*3.48*	*1.57*	*0.62*	*2.74*		*3.76*		*2.50*		*2.39*	

Table 5. continued

Sample No	La	Ce	Pr	Nd	Sm	Eu	Gd	Tb	Dy	Ho	Er	Tm	Yb	Lu
Keldysh/Mir 90														
M-2212-2	3.495	9.406	1.542	7.647	2.593	0.937	3.442	0.644	3.980	0.886	2.618		2.404	0.365
M-2212-2g	3.241	8.975	1.426	7.398	2.404	0.874	3.166	0.577	3.601	0.793	2.296		2.097	0.308
M-2218-1	4.165	9.982	1.780	7.855	2.855	1.028	3.984	0.724	4.900	1.071	3.117	0.473	2.718	0.454
M-2218-2	3.740	10.410	1.651	8.491	2.755	0.934	3.480	0.632	3.882	0.854	2.412		2.160	0.316
	4.523	10.517	1.750	8.132	2.874	1.070	4.152	0.748	4.935	1.062	3.142	0.457	0.288	0.468
M-2218-3	4.157	10.187	1.717	7.825	2.803	1.085	3.717	0.701	4.259	0.893	2.805	0.400	2.652	0.426
M-2218-4														
M-2218-4g	3.351	9.630	1.603	8.235	2.755	1.009	3.673	0.678	4.314	0.955	2.804		2.586	0.384
M-2218-7	5.879	14.261	2.430	10.657	3.587	1.387	5.440	0.903	6.191	1.368	4.027	0.623	3.505	0.648
M-2218-8														
M-2218-9	3.305	9.493	1.545	8.036	2.651	0.981	3.508	0.658	4.078	0.900	2.609		2.397	0.354
M-2218-10	3.258	9.100	1.483	7.478	2.501	0.938	3.375	0.643	3.987	0.879	2.623		2.420	0.365
M-2218-11	3.4635	8.7117	1.3741	6.7319	2.4758	0.9091	3.414	0.5932	3.9057	0.8628	2.5199	0.355	2.4417	0.3984
M-2218-12	5.814	14.584	2.493	11.307	3.570	1.268	5.243	1.017	6.212	1.351	3.721	0.535	3.672	0.621
Melville 96														
113-1-12	2.304	4.07	0.52	2.271	0.62	0.239	0.75	0.126	0.814	0.196	0.584		0.652	0.106
113-1-32	2.57	4.816	0.728	3.673	1.224	0.332	1.79	0.344	2.348	0.561	1.658		1.795	0.296
115-1-1	1.431	2.182	0.29	1.251	0.349	0.126	0.43	0.073	0.463	0.109	0.339		0.373	0.061
115-2-7	2.398	4.527	0.6	2.768	0.768	0.3	0.98	0.178	1.132	0.269	0.786		0.889	0.146
116-1-3	9.244	18.815	2.459	10.999	2.741	0.839	2.95	0.497	3.105	0.694	1.974		2.15	0.351
117-2-3	12.163	23.892	3.101	13.374	3.118	0.926	3.35	0.563	3.434	0.766	2.248		2.446	0.399
118-2-5	13.892	26.08	3.01	11.868	2.358	0.659	2.16	0.35	2.075	0.45	1.352		1.501	0.247
119-1-1	5.787	11.582	1.45	6.033	1.268	0.421	1.28	0.201	1.09	0.236	0.644		0.667	0.104
119-2-5	3.712	6.321	0.711	2.848	0.645	0.224	0.76	0.138	0.843	0.194	0.601		0.642	0.106
120-1-1	9.813	20.82	2.757	12.252	2.965	1.009	3.19	0.543	3.206	0.678	1.92		1.89	0.296
120-2-1	10.138	20.541	2.66	11.676	2.827	0.956	3.05	0.516	3.054	0.653	1.81		1.84	0.285

Table 5. continued

Sample No	Hf	Ta	Pb	Th	U
Kallisto 82					
16-9/1	3.900	2.425	5.727	6.096	1.609
16-10/4	4.224	2.711	5.210	4.175	1.267
16-94/1	6.119	2.742	4.929	4.342	1.215
16-26/1	0.469	0.207	1.345	0.577	0.185
16-26/2	0.509	0.261	1.327	0.713	0.202
Natsushima 84					
7-18	1.173	0.878	3.086	2.109	0.596
6-3	0.806	0.483	1.995	0.893	0.259
5-25	0.558		0.819	0.089	0.065
	0.562		0.733	0.079	0.065
5-24	0.193	0.028	0.727	0.041	0.038
	0.188		0.608	0.028	0.033
5-28	0.205		0.620	0.028	0.033
5-27	0.760	0.061	0.930	0.111	0.086
5-20	1.092	0.084	1.255	0.174	0.116
	1.102		0.890	0.142	0.100
3-44	0.372	0.084	1.813	0.327	0.156
3-51	0.396	0.067	1.259	0.339	0.176
3-24	0.592	0.086	2.580	0.600	0.246
3-36	1.204	0.218	5.012	2.078	0.694
11-3					

Table 5. continued.

Sample No	Hf	Ta	Pb	Th	U
Keldysh/Mir 90					
M-2212-2	1.574	0.151	1.098	0.315	0.135
			0.660	0.470	0.330
M-2212-2g	1.609	0.186	0.804	0.247	0.117
M-2218-1			2.310	0.420	0.190
M-2218-2	1.946	0.187	0.923	0.283	0.129
			0.480	0.460	0.210
M-2218-3			1.650	0.870	0.670
M-2218-4			0.540	0.280	0.080
M-2218-4g	1.808	0.154	0.940	0.221	0.076
M-2218-7			2.100	0.680	0.290
M-2218-8			1.150	0.460	0.280
M-2218-9	1.792	0.156	1.074	0.212	0.080
			0.590	0.160	0.050
M-2218-10	1.592	0.139	0.806	0.261	0.120
			0.630	0.350	0.150
M-2218-11			0.110	0.360	0.120
M-2218-12			1.250	0.570	0.390
Melville 96					
113-1-12	0.373		2.66	0.369	0.197
113-1-32	1.183		1.81	0.438	0.261
115-1-1	0.21		1.01	0.232	0.089
115-2-7	0.469		1.53	0.446	0.159
116-1-3	1.665		3.03	1.519	0.575
117-2-3	2.182		5.01	2.021	0.732
118-2-5	1.988		5.31	2.47	0.875
119-1-1	0.601		1.24	0.908	0.263
119-2-5	0.451		1.33	0.842	0.261
120-1-1	1.849		1.6	1.371	0.475
120-2-1	1.74		2.16	1.421	0.435

Table 6. Isotope geochemistry of rock samples dredged from the northern Lau – Tonga area

sample	lab	$^{87}Sr/^{86}Sr$	$^{143}Nd/^{144}Nd$	$^{206}Pb/^{204}Pb$	$^{207}Pb/^{204}Pb$	$^{208}Pb/^{204}Pb$
Kallisto 82						
16-9/1	MELB	0.704155	0.512757	19.215	15.644	39.154
16-10/4	MELB	0.704299	0.512743	19.143	15.632	39.064
Natsushima 84						
5-24	MELB	0.704465	0.512977	18.625	15.570	38.435
	MELB			18.623	15.569	38.431
	MELB	0.704404	0.512979			
	MELB	0.704439	0.512964			
5-28	MELB	0.704439	0.512959	18.639	15.566	38.450
5-20	ANU			18.583	15.541	38.329
3-24	ANU			18.740	15.585	38.676
3-22	ANU			18.757	15.575	38.711
3-52	ANU			18.795	15.583	38.748
3-36	ANU			18.827	15.596	38.789
11-3	ANU			18.074	15.503	38.117
Melville 96						
113-1-12	MELB	0.704825	0.512810	18.879	15.591	38.788
115-1-1	MELB	0.704603	0.512812	18.766	15.591	38.717
115-2-7	ADEL	0.704443	0.512780			
116-1-3	MELB	0.704076	0.512865	19.229	15.616	38.940
	MELB			19.225	15.614	38.933
118-2-5	ADEL	0.704378	0.512714			
119-2-5	MELB	0.704884	0.512755	18.883	15.619	38.911
	MELB	0.704849	0.512760	18.874	15.620	38.897
120-1-1	MELB	0.703839	0.512861	19.026	15.602	38.908

Table 7. End-Member Compositions for the Mixing Calculations Discussed in the Text

	Altered Oceanic Crust Fluid	ODP834	Cook-Austral Plume	Peggy Ridge	Uo Mamae	Depleted Boninite	Upolu PE	Kallisto 16-9/10
$^{87}Sr/^{86}Sr$	0.704465-0.704047	0.702618	0.70499	0.702936	0.705183	0.704465	0.705492	0.704299
$^{143}Nd/^{144}Nd$	0.512977-0.512961	0.513125	0.512787	0.513181	0.51248	0.512977	0.512618	0.512743
Sr (ppm)	2380	186	367	12	705.2	47.6	861	862
Nd (ppm)	39.7	14.18	42.3	0.64	39.988	0.794	55.86	49.6

APPENDIX 1. Petrographic summary of samples studied.

Petrographic Group	Samples	Comments
Olivine + orthopyroxene ± clinopyroxene ± plagioclase – phyric Boninite	113-1-24, 113-1-30, 113-1-12	Carbonate-altered intrusive holocrystalline boninite with large opx phenocrysts, and carbonate-altered former oliv phenocrysts. The groundmass lacks glass, and is an intergrowth of opx and cpx microlites. Opx psuedomorphed by chlorite, and a few small phenoccrysts by microcrystalline silica. Smectite/chlorite±zeolite alteration of the groundmass with common tiny FeTi oxides.
Orthopyroxene + clinopyroxene ± olivine – phyric Boninite	115-1-1,115-1-2,115-1-8,115-1-10,115-1-11,115-1-5	Strongly porphyritic vesicular boninitic high-Mg andesite dominated by large opx and cpx phenocrysts, with abundant evidence of magma mixing, including partially reacted grains, opx with strong reverse zoned rims. Very little chromite.
Orthopyroxene + plagioclase ± clinopyroxene – phyric Andesite	115-2-5,115-2-7	
Orthopyroxene + clinopyroxene + plagioclase + titanomagnetite ± apatite – phyric Dacite	116-1-1,116-1-3	Highly vesicular, glassy
Plagioclase + orthopyroxene + clinopyroxene + titanomagnetite + apatite – phyric Rhyolite	117-1-1,117-2-3	Vesicular, glassy groundmass
Plagioclase + quartz + orthopyroxene + clinopyroxene + titanomagnetite – phyric Rhyolite	118-2-5,118-2-8	Massive, vesicular, glassy groundmass
Olivine + orthopyroxene + Cr-spinel ± clinopyroxene – phyric Boninite	119-1-1,119-2-5,119-3-5,119-3-6	Vesicular and strongly to moderately porphyritic very fresh boninite with common large oliv and opx phenocrysts, in a quenched groundmass of glass charged with small cpx and opx microlites. Samples 119-3-5, -6 are sparsely phyric to aphyric.
Olivine + plagioclase + clinopyroxene – phyric Basalts	120-1-1,120-1-3,120-2-1,120-2-3	Both pillow and tabular pahoehoe pieces

APPENDIX 2. Selected mineral analyses

Sample	Mineral	Type	Analysis No.	SiO_2	TiO_2	Al_2O_3	Cr_2O_3	FeO	MnO	MgO	CaO	Na_2O	K_2O	NiO	Mg#	An
113-1-24	Plag	Ph	50	48.08		31.79		1.36		0.18	16.56	1.98	0.04			82.0
	Cpx	Ph	62	52.35	0.15	1.63	0.21	7.95	0.25	17.42	19.93	0.11			79.6	
	Opx	Ph	59	55.52	0.07	1.05	0.44	8.94	0.22	31.92	1.82	0.01			86.4	
	Opx	mPh	56	54.49	0.08	1.51	0.04	12.28	0.32	29.39	1.87	0.03			81.0	
115-1-8	Cpx	Ph	24	52.81	0.06	1.56	0.48	7.95	0.22	17.13	19.71	0.08			79.3	
	Opx	Ph	27	54.92	0.03	0.93	0.14	14.30	0.36	27.08	2.24	0.01			77.1	
	Opx	Ph	28	56.55	0.00	0.40	0.24	9.18	0.22	31.14	2.24	0.02			85.8	
115-1-10	Plag	mcl	17	47.51		30.09		2.46		0.50	17.07	2.20	0.17			80.3
	Cpx	Ph	23	53.60	0.03	0.54	0.56	5.03	0.21	19.35	20.56	0.12			87.3	
	Cpx	Ph	22	51.60	0.06	1.34	0.24	8.50	0.26	17.97	19.94	0.08			79.0	
	Opx	Ph	16	52.23	0.03	1.25	0.14	16.24	0.45	27.45	2.17	0.04			75.1	
115-1-11	Oliv	Ph	29	38.79			0.01	13.65	0.27	47.00	0.20			0.08	86.0	
	Opx	Ph	28	53.29	0.04	0.97	0.08	15.27	0.47	27.67	2.22	0.01			76.4	
	Cpx	Ph	25	52.72	0.06	1.49	0.16	8.34	0.33	17.28	19.55	0.08			78.7	
115-2-5	Opx	Ph	20	54.58	0.07	0.93	0.06	16.87	0.43	24.80	2.24	0.02			72.4	
	Plag	Ph	24	44.28		34.55		0.68		0.06	19.72	0.68	0.03			94.0
116-1-1	Cpx	mPh	41	51.44	0.28	1.85	0.01	11.55	0.41	14.61	19.69	0.16			69.3	
	Opx	mPh	44	52.73	0.24	1.04	0.00	22.35	0.80	20.87	1.95	0.02			62.5	
	Plag	mPh	39	55.64		26.81		1.60		0.15	11.79	3.79	0.23			62.3
	Ti-mag	mPh	43	0.23	7.02	3.42	0.00	87.62	0.31	1.37	0.02					

APPENDIX 2. Selected mineral analyses continued

Sample	Mineral	Type	Analysis No.	SiO_2	TiO_2	Al_2O_3	Cr_2O_3	FeO	MnO	MgO	CaO	Na_2O	K_2O	NiO	Mg#	An
116-3-1	Opx	Ph rim	30	53.38	0.16	0.95	0.05	20.71	0.50	22.30	1.89	0.06			65.7	
	Cpx	Ph	38	51.18	0.32	1.90	0.04	11.87	0.37	13.98	20.09	0.24			67.7	
	Plag	Ph	43	47.73		32.37		0.99		0.11	16.91	1.85	0.04			83.3
	Ti-mag	mPh	37	0.10	6.16	3.26	0.11	87.99	0.24	2.14	0.00					
117-2-3	Cpx	Ph	4	51.00	0.26	0.98	0.00	16.50	0.53	11.45	19.14	0.15			55.3	
	Opx	Ph	30	50.41	0.24	0.65	0.01	31.22	0.90	14.64	1.94	0.00			45.5	
	Plag	Ph	3	50.21		31.03		0.61		0.03	15.12	2.94	0.06			73.7
	Ti-mag	mPh		0.12	15.28	1.97	0.03	80.94	0.54	1.11	0.01					
118-2-8	Opx	Ph	11	52.71	0.17	0.51	0.02	24.16	0.60	20.51	1.30	0.02			60.2	
	Cpx	Ph	20	51.96	0.21	0.97	0.00	11.38	0.36	13.65	21.28	0.19			68.1	
	Plag	Ph	52	48.20		32.41		0.58		0.03	16.19	2.53	0.06			77.7
	Ti-mag	mPh	25	0.11	8.67	2.15	0.23	87.15	0.31	1.30	0.08					
119-1-1	Cpx	Ph r	6	54.04	0.14	1.18	0.57	4.01	0.11	19.05	20.78	0.11			89.4	
	Oliv	Ph r	19	41.23			0.14	7.03	0.10	50.99	0.21			0.31	92.8	
	Oliv	Ph c	18	40.69			0.05	10.45	0.14	48.16	0.31			0.21	89.1	
	Cr-sp	incl	21	0.08	0.33	9.76	58.59	16.82	0.22	14.21	0.00					
120-1-1	Oliv	Ph	64	38.79				18.78	0.31	41.75	0.27			0.11	79.8	
120-1-3	Oliv	mPh	47	38.71				17.62	0.29	43.02	0.20			0.16	81.3	
120-1-1	Plag	Ph	60	49.33		31.22		0.78		0.26	15.63	2.68	0.10			75.9
120-1-1	Plag	Ph	61	46.19		33.66		0.55		0.14	18.05	1.36	0.04			87.8
120-2-3	Plag	Ph c	23	44.40		34.99		0.57		0.12	18.98	0.92	0.02			91.8
120-1-1	Cpx	Ph	59	52.19	0.38	2.09	0.07	6.78	0.18	17.75	20.45	0.13			82.3	
120-2-1	Cpx	mPh	17	50.21	0.81	5.00	0.10	8.13	0.22	16.11	19.24	0.18			77.9	
120-2-1	Cpx	mPh	19	50.92	0.63	4.07	0.15	7.13	0.34	16.51	20.09	0.17			80.5	

Appendix 3. The correct Table 2 from *Falloon and Crawford* [1991], giving the major and trace element geochemistry for station 21 high-Ca boninite lavas, northern Tonga (see *Falloon and Crawford*, [1991] for other details)

Group	I	I	II	II	II	III	III	III	III	IV	IV	IV	IV
Sample No	D3-44	D3-39	D3-21	D3-51	D3-49	D3-45	D3-47	D3-25	D3-46	D3-53	D3-22	D3-34	D3-41
SiO_2	54.35	54.53	54.35	53.95	52.41	55.39	55.18	55.79	55.58	57.51	56.01	59.06	55.84
TiO_2	0.2	0.22	0.23	0.23	0.21	0.29	0.31	0.3	0.24	0.29	0.29	0.34	0.33
Al_2O_3	10.67	11.43	12.88	12.88	11.12	10.85	10.94	11.45	10.58	13.18	13.88	13.29	14.47
FeO	9.41	9.3	9.88	9.81	9.54	9.87	10	9.87	9.96	9.22	9.7	9.23	9.84
MnO	0.19	0.18	0.16	0.16	0.18	0.18	0.19	0.18	0.19	0.18	0.19	0.18	0.19
MgO	14.99	13.34	10.59	10.4	14.87	12.05	12.14	11.08	12.54	8.14	7.78	6.26	6.93
CaO	8.66	9.53	9.87	10.5	9.99	9.36	9.24	9.29	9.48	9.53	9.98	9.13	9.98
Na_2O	1.14	1.09	1.56	1.6	1.41	1.48	1.48	1.42	1.03	1.35	1.63	1.78	1.74
K_2O	0.35	0.34	0.44	0.45	0.2	0.48	0.48	0.58	0.36	0.54	0.47	0.64	0.61
P_2O_5	0.03	0.03	0.04	0.03	0.05	0.05	0.05	0.05	0.04	0.06	0.06	0.09	0.07
LOI	0.05	0.36	1.07	1.33	1.46	0.59	0.98	1.08	0.28	-0.07	-0.15	-0.04	0.5
Ba	106	86	112	104	98	108	113	117	93	140	131	163	161
Rb	6	7	4	5	2	7	7	9	5	8	7	10	12
Sr	151	161	172	175	264	177	172	190	156	202	236	223	271
Zr	12	11	10	9	9	18	20	18	11	17	14	19	18
Nb		2				1		1		1	1		1
Y	7	7	5	6	8	9	8	10	8	9	10	11	9
Sc	50	51	48	53	45	48	51	46	53	50	49	47	47
V	247	261	326	343	253	247	259	252	256	275	281	275	292
Ni	275	215	122	123	233	150	153	132	143	84	78	47	67
Cr	1095	814	435	445	935	729	762	607	774	365	281	196	196
Hf	0.61			0.3			0.55			0.6	0.72		
Ta	<0.3			<0.3			<0.3			<0.3	<0.3		
Th	0.48			0.54			0.53			0.82	0.47		

Appendix 3. continued

Group	IV	IV	IV	IV	IV	V	VI	VI	VI	VI	VI	VI	VI
Sample No	D3-28	D3-52	D3-40	D3-26	D3-31	D3-24	D3-27	D3-36	D3-30	D3-23	D3-29	D3-32	D3-42
SiO_2	54.4	56.77	56.74	55.66	57.27	59.19	55.59	60.17	60.8	59.81	60.19	60.01	60.73
TiO_2	0.27	0.3	0.34	0.3	0.34	0.25	0.31	0.42	0.43	0.41	0.42	0.41	0.43
Al_2O_3	14.81	14.59	16.18	15.31	15.39	10.96	15.51	15.21	14.95	15.3	15.2	15.32	15.27
FeO	10.02	9.32	9.38	9.61	9.34	8.83	9.82	8.9	8.72	8.82	8.94	8.88	8.7
MnO	0.17	0.18	0.15	0.17	0.17	0.18	0.17	0.15	0.15	0.14	0.14	0.15	0.14
MgO	7.82	6.42	4.55	6.39	5.15	10.8	6.01	3.35	3.11	3.34	3.33	3.35	3.14
CaO	10.69	10.35	9.95	10.57	9.72	7.78	10.71	7.68	7.48	7.65	7.67	7.64	7.45
Na_2O	1.38	1.52	1.98	1.45	1.86	1.37	1.41	2.96	2.86	3.16	2.79	2.85	2.99
K_2O	0.4	0.46	0.64	0.47	0.67	0.56	0.43	1.01	1.35	1.21	1.17	1.24	0.99
P_2O_5	0.04	0.09	0.09	0.06	0.08	0.07	0.04	0.14	0.14	0.14	0.14	0.14	0.15
LOI	0.04	0.03	0.04	0.45	0.13	0.01	0.3	0.83	2.23	2.04	1.73	2.02	-0.03
Ba	107	116	180	123	170	140	104	271	278	268	270	267	274
Rb	8	10	9	8	12	10	7	19	21	20	21	20	13
Sr	189	206	319	212	260	175	196	385	379	387	389	384	396
Zr	15	14	20	16	23	19	16	44	41	40	43	40	41
Nb	1	2	1	2	2	2	2	4	4	4	5	3	3
Y	8	8	11	10	11	7	9	13	12	12	12	13	14
Sc	51	52	42	50	45	43	52	34	32	33	32	32	32
V	323	338	288	345	333	251	330	309	274	305	310	307	247
Ni	99	63	40	64	43	117	50	21	16	19	19	17	18
Cr	287	180	88	159	94	605	78	17	17	14	13	13	16
Hf		0.48				0.84	0.9	1.51					
Ta		<0.3				<0.3	<0.3	<0.3					
Th		0.62				0.9	0.7	2.3					